ChemEurJ

Research Article
doi.org/10.1002/chem.202501864

Chemistry Europe
European Chemical Societies Publishing

www.chemeurj.org

Tuning NIR Absorption and Emission of Diphenyl-Dihydrophenazine-Based Merocyanines with Ultra Narrow Band Gap

Kateřina Teichmanová,[a, b] Stanislav Luňák Jr.,[c] Karel Pauk,[b] Lukáš Střižík,[d] Zdeňka Růžičková,[d] Tomáš Mikysek,[e] Klára Melánová,[f] Aleš Imramovský,*[b] and Kazuhiko Nagura*[a]

Five merocyanine derivatives with a 5,10-diphenyl-dihydrophenazine donor and various indanone-and indandione based-acceptors with one or two dicyanovinylene groups were prepared by Knoevenagel condensation for tuning absorption and fluorescence in the near-infrared region. Molecular conformation, bond length alternation, and molecular packing in the solid state were studied by X-ray diffraction of single crystals in combination with density functional theory (DFT) calculations. By enhancing electron-accepting ability, a considerable decrease of lowest unoccupied molecular orbitals (LUMO) energy by 1.01 eV and retained highest occupied molecular orbitals (HOMO) energy within 0.13 eV were estimated by cyclic and rotating disc electrode voltammetry, relating semi-quantitatively to DFT prediction. Optical properties in solutions with various polarity, neat amorphous films, and crystalline powder states were studied. The absorption maxima of the neat films evolved from 545 nm to 931 nm. An ultranarrow optical band gap of DPPZ-IDD (1.09 eV) was found from the onset of thin film absorption and well agreed with the electrochemical gap of 0.93 eV. Detectable fluorescence in the NIR region was observed in the film and polycrystalline powder states.

1. Introduction

The solar light falling on the Earth's surface covers a wide spectral range from ultraviolet (UV, 250 nm–380 nm) over visible (Vis, 380 nm–740 nm) to infrared (IR, 740 nm–2500 nm).[1] The absorption threshold of materials is given by an optical band gap (E_g), that is, the difference between the highest occupied (HOMO) and lowest unoccupied molecular orbitals (LUMO) energy levels. Besides other physical properties, such as high absorptivity, exciton dynamics, and charge transfer ability, materials utilizing infrared radiation effectively (e.g., in organic photovoltaics (OPV)) must have at least a narrow band gap (E_g = 1.6 eV–1.3 eV)[2] or even an ultra-narrow band gap (E_g < 1.3 eV).[3] On the other hand, the materials for biological imaging and therapeutics (theranostics) emitting over 1000 nm are of great importance,[4,5] because biological tissues are more transparent and scatter less in so-called NIR I (650–1000 nm) and especially NIR II (1000 nm–1700 nm) spectral windows.[6] Besides the above-mentioned utilities, the applications like infrared detectors,[7] NIR Organic Light-Emitting Diodes (OLEDs),[8] NIR solid-state lasers[9] and the materials for photoacoustic bioimaging[10] are hot topics of scientific research. Thus, the development of new-infrared absorbing and emitting organic dyes is of general importance.

Except for exotic chromophores with an open electronic shell,[11] typical organic NIR chromophores and fluorophores can be classified as ionic (e.g., cyanines, rhodamines), intraionic

[a] K. Teichmanová, K. Nagura
Research Center for Materials Nanoarchitectonics (MANA), National Institute for Materials Science, 1-1 Namiki, Tsukuba, Ibaraki 304-0044, Japan
E-mail: nagura.kazuhiko@nims.go.jp

[b] K. Teichmanová, K. Pauk, A. Imramovský
Institute of Organic Chemistry and Technology, Faculty of Chemical Technology, University of Pardubice, Studentská 95, Pardubice 53009, Czech Republic
E-mail: ales.imramovsky@upce.cz

[c] S. Luňák Jr.
Materials Research Centre, Faculty of Chemistry, University of Technology, Purkyňova 464/118, Brno 61200, Czech Republic

[d] L. Střižík, Z. Růžičková
Department of General and Inorganic Chemistry, Faculty of Chemical Technology, University of Pardubice, Studentská 95, Pardubice 53009, Czech Republic

[e] T. Mikysek
Department of Analytical Chemistry, Faculty of Chemical Technology, University of Pardubice, Studentská 95, Pardubice 53009, Czech Republic

[f] K. Melánová
Center of Materials and Nanotechnologies, Faculty of Chemical Technology, University of Pardubice, Studentská 95, Pardubice 53009, Czech Republic

Supporting information for this article is available on the WWW under https://doi.org/10.1002/chem.202501864

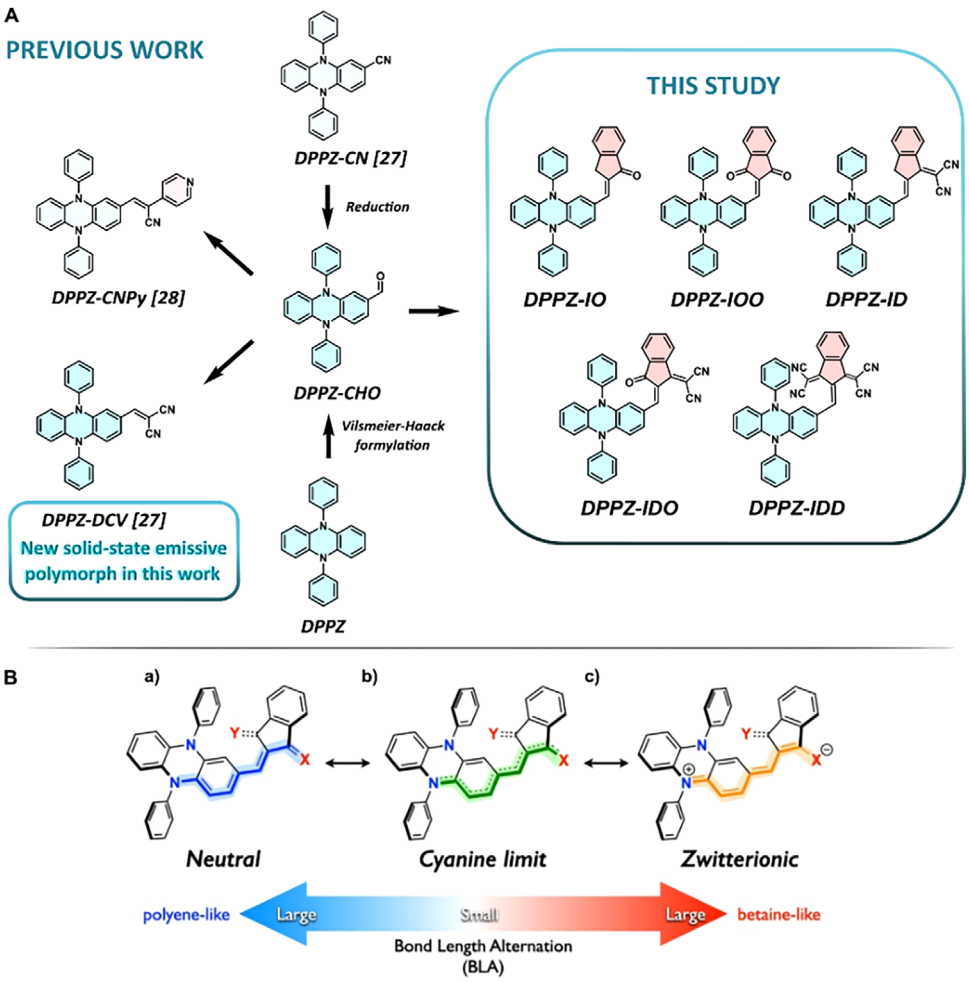

Figure 1. A) Previous and current synthetic approaches to **DPPZ-EWG** derivatives, together with the nomenclature of the compounds in this study. B) Graphical representation and bond length alternation tendency of **DPPZ-EWG** for A) neutral form, B) cyanine limit as an intermediate, and (c) zwitterionic form.

(e.g., squaraines, BODIPY), or coordination complex (e.g., phthalocyanines).[12] Widely employed molecular design strategies for neutral molecules to achieve a bathochromic shift in absorption and fluorescence are conjugation extension[13] and intramolecular charge transfer (ICT) between electron-donating (D) and electron-accepting (A) groups through a conjugated bridge (π).[14] If considering all three molecular components (D, π, A) separately, their changes enable tuning of the energies of both frontier orbitals. Typically, an increasing strength of a donor part mainly destabilizes HOMO of a molecule, raising the strength of an acceptor moiety stabilizes LUMO, and conjugation extension may support both trends. Furthermore, the absolute HOMO and LUMO energy levels of materials in electronic devices like OPV cells or OLEDs must be harmonized with the energy levels of other components of a device, which complicates achieving the required narrow band gap.[3b] Besides the simplest D-π-A arrangement, quadrupolar A-π-D-π-A architectures are popular in organic photovoltaic materials as various modifications of ITIC and Y6 electron acceptors.[15] The 3-dicyanomethylene-indanone (**IDO** in our nomenclature in Figure 1) unit is typically used as a terminal electron-withdrawing group (EWG) in these nonfullerene electron acceptors.[2] On the other hand, compounds with D-π-A-π-D architecture are more frequently used in the OLEDs area, because of their ability to emit in the NIR region in solid state.[8]

Merocyanines are a special class of D-π-A chromophores with usually a polymethine chain, typically an amine donor and a carbonyl acceptor.[16] Polymethine dyes are characterized by an odd number of methine (sp^2 hybridized) centers and an even number of π-electrons.[17] Optical and electronic properties of merocyanines are usually interpreted via the contribution of neutral and zwitterionic resonance structures. The formation of centrosymmetric antiparallel stacks by strong electrostatic interactions is frequently observed in the crystalline state and is often considered as a main reason for the absence of solid-state fluorescence.[18] Among merocyanines derivatives, styryl dyes (streptomerocyanines) are categorized as a distinct subclass with a styryl unit and an even number of π-electrons distributed over an odd number of π-centers between D and A.[17b] Typically, they are prepared by Knoevenagel condensation of 4-amino-arylaldehyde with active methylene compounds. Regioisomeric styryl dyes with an amino donor at *meta* position fall outside

the definition of streptomerocyanines because of an even number of π-centers between D and A. Therefore, these *meta* chromophores show a bathochromic shift of the longest absorption maximum with a smaller molar coefficient and red-shifted fluorescence compared to the *para* chromophores.[19]

Free-rotating propeller-like triarylamines and partially fixed 9-aryl-carbazoles are frequently used as terminal electron-donating groups. For emitting DA derivatives, the combination of these donor groups with a sufficiently strong acceptor can induce solid-state fluorescence (SSF) in the NIR I region.[20] Furthermore, the bridging of the triphenylamine core by heteroatoms including oxygen, sulphur, and nitrogen atoms can enhance the donating ability and cause a red shift in absorption and fluorescence spectra.[21] Among them, symmetrical 5,10-diphenyl-dihydrophenazine (DPPZ) is an electron-rich unit with a high HOMO level.[22] Symmetrically modified DPPZ derivatives with aryl substitutions at positions 5 and 10 have demonstrated enhanced solid-state emission[23] and thermally activated delayed fluorescence[24] as well as stable radical cations formation,[25] singlet oxygen generation[24] and efficient photocatalytic activity.[26] An absorption of the reported DPPZ derivatives always falls into the visible region and their fluorescence sometimes achieves between Vis and NIR borderline.[24] Direct introduction of strong EWG on dihydrophenazine core to form asymmetrical DA compounds is limited to dicyanovinylene (DCV)[27] and cyanopyridine-vinylene[28] (Figure 1). However, this strategy has the potential to shift fluorescence maximum further, as observed for **DPPZ-DCV** nanoparticles (700 nm).

Previously we had developed a series of D-π-A-type stilbene derivatives for SSF. We succeeded in tuning fluorescence colors from visible to NIR regions by introducing diphenylamino donor and various EWG and by controlling the polymorphism in the crystalline states.[29] To develop novel chromophores with narrow band gap and fluorophore in the NIR regions, we designed a series of merocyanine derivatives with strong **DPPZ** donor and indanone-based acceptors (Figure 1A). We systematically investigated the LUMO energy levels of the indanone acceptor units by modifying the number of terminal EWG with the expected sequence from IO < IOO <ID < IDO < IDD.[30] Although the effect of these units comes from a complicated influence of (branched) conjugation extension and heterosubstitutions, considering them as the complex acceptors on styryl conjugated bridge appeared sufficient for the interpretation of experimental results in most cases. We envisioned that this acceptor modification affects the balance between neutral and zwitterionic electronic structure of the merocyanine skeleton as well as their optical and electronic properties. Here, to reveal these structure–property relationships and the intrinsic effect of *meta* nitrogen atom of DPPZ toward the merocyanine skeleton, we have established synthetic routes for this series. Their molecular geometry and packing structure in crystalline state were characterized by X-ray diffraction (XRD). Their electrochemical properties as well as HOMO and LUMO energy levels were estimated by cyclic voltammetry (CV) and rotating disk electrode voltammetry (RDEV). Furthermore, their optical properties, including absorption and fluorescence spectra in various environments, were investigated in conjugation with quantum chemical calculations based on density functional theory (DFT) and time-dependent (TD) DFT calculations.

2. Results and Discussion

The preparation of the target molecules **DPPZ-EWG** began with the synthesis of the key intermediate **DPPZ-CHO**. Previously, **DPPZ-CHO** was obtained through a two-step process starting from a condensation of *N,N*-diphenylbenzene-1,2-diamine and 3,4-difluorobenzonitrile in the presence of sodium hydride followed by reduction of nitrile with diisopropylaluminium hydride.[27] A direct method for preparing the monoaldehyde derived from the *N,N*-dimethyl-dihydrophenazine has been only partially described.[31] In contrast, our novel approach to **DPPZ-CHO** was carried out according to Scheme 1 from commonly available, safe, and inexpensive starting compounds. Phenazine was first reduced by sodium dithionite with quantitative yield, according to literature.[25c] Arylation of obtained 5,10-dihydrophenazine using Buchwald-Hartwig amination in the presence of a Pd catalyst afforded *N,N*-diphenyl-5,10-dihydrophenazine (**DPPZ**) in a moderate yield of 52%.[32] As a direct formylation approach, a straight and industrially applicable method of Vilsmeier-Haack formylation provided **DPPZ-CHO** as the major product (63% isolated yield). **DPPZ-CHO** was further converted into six **DPPZ-EWG** derivatives containing different acceptor groups with increasing electron-withdrawing ability. To improve the electron-accepting properties, one or both carbonyl groups in 1-indanone (**IO**) and indane-1,3-dione (**IOO**) were selectively functionalized by malononitrile in the presence of sodium acetate.[33] Knoevenagel condensations between the aldehyde group of **DPPZ-CHO** and the activated methylene group of acceptors were performed in the presence of pyridine or piperidine as a base, except for compounds **DPPZ-IO** and **DPPZ-IDD**. For **DPPZ-IDD,** an optimized acidic media in acetic anhydride was necessary because of the high stability of the deprotonated intermediate **IDD**$^-$ without enough nucleophilicity under basic conditions.[33] All target compounds were purified by column chromatography, recycling high-performance liquid chromatography (HPLC), and subsequent recrystallization. Their molecular structures were confirmed by ^{1}H, ^{13}C NMR, and high-resolution mass spectrometry (HRMS).

Most of the compounds in this study formed single crystals suitable for X-ray crystallographic analysis (Figure S1). Crystals of **DPPZ-CHO** were formed as twins, which led to the static disorder treated by standard operations and attributing electron maxima to pairs of atoms with occupancy of 66/34. Two polymorphs of **DPPZ-DCV** were obtained: the reported polymorph was obtained from ethyl acetate,[27] while the new polymorph was crystallized from either $CHCl_3$ or CH_2Cl_2. The solvent molecules ($CHCl_3$) were present within the crystal structures of **DPPZ-DCV** (parallel), **DPPZ-IO,** and **DPPZ-IOO**. Merocyanines with only carbonyl acceptor often tend to accommodate solvents into crystal lattice.[34] Except major prismatic crystals of **DPPZ-IOO** included $CHCl_3$ via the weak hydrogen bond between chloroform C—H and O═C of acceptors, further needle crystals could be manually separated from the crystallization crop. The conformation and

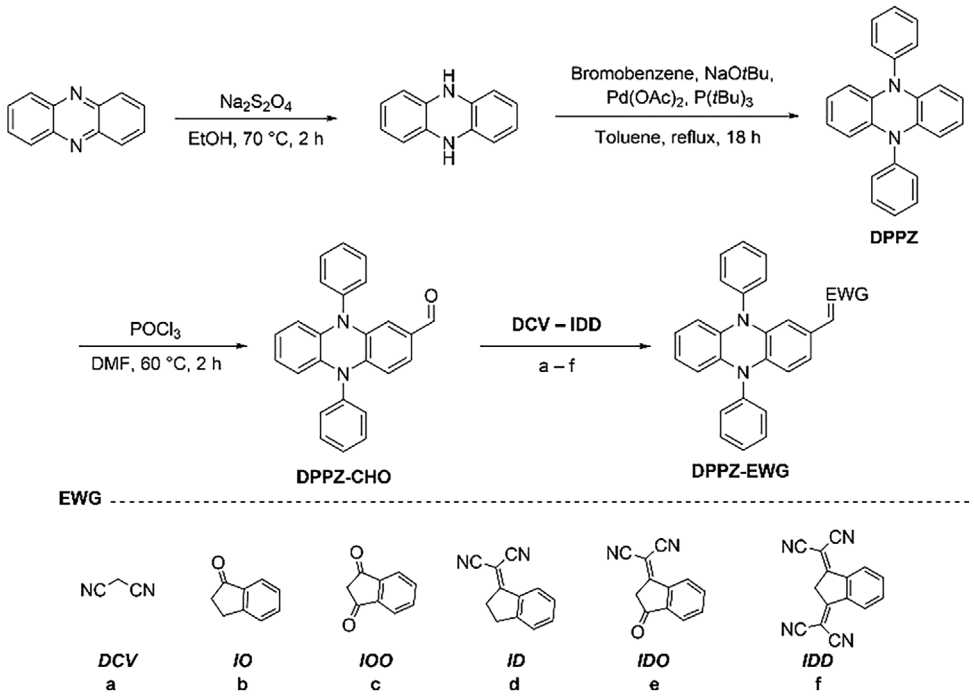

Scheme 1. Synthetic route of **DPPZ-EWG**. Reaction conditions: A) malononitrile, piperidine, CH_2Cl_2, RT, 20 minutes; B) 1-indanone, 6M NaOH, $CHCl_3$, rt, 18 hours; C) indan-1,3-dione, piperidine, ethanol, reflux, 18 hours; D) ID, piperidine, toluene, reflux, 18 hours; E) IDO, pyridine, ethanol, reflux, 18 hours; F) IDD, Ac_2O, reflux, 5 minutes.

packing arrangement of the needle crystals of **DPPZ-IOO** were similar to those of prismatic crystals of **DPPZ-IO** where the chloroform C—H directed toward the electron-rich dihydrophenazine ring A (Figure 2). Solvent-free crystals of **DPPZ-ID** and **DPPZ-IDO** were obtained from ethyl acetate. Unfortunately, the attempts to obtain single crystals of **DPPZ-IDD** suitable for single-crystal XRD failed. The crystallographic parameters are summarized in Tables S1–S7, data are stored within the CSD (Nos. 2434164–2434170).

To obtain structural insights about conformation and bond length alternation (BLA) in solution state, we conducted DFT calculations of **DPPZ-EWG**. The optimized structures in solution state were estimated at the CAM-B3LYP/6-311G(d,p) with $CHCl_3$ involved through polarizable continuum models (PCM) (Figure S3). Monomethine merocyanines **DPPZ-EWG** may exist in either *s-trans* or *s-cis* conformation with respect to the exocyclic single bond in neutral form.[35] The differences in the calculated energies of both conformers are comparable (Table 1), *s-cis* conformations are thermodynamically a bit more stable than *s-trans* conformations for all derivatives. The calculated energy barriers with respect to φ_1 rotation are slightly higher (e.g., ~9.0 kcal·mol^{-1} for **DPPZ-IOO** and ~7.4 kcal·mol^{-1} for **DPPZ-IDO**) than that of a conventional single bond but are not high enough to prevent a thermal equilibrization of both conformers in the ground state. Thus ^{1}H NMR spectrum of **DPPZ-EWG** indicated averaged structures of rotamers at room temperature. DFT calculations imply perfectly coplanar dihydrophenazine donor, methine bridge, and acceptor, and exactly perpendicular side phenyls C and D for **DPPZ-CHO**, **DPPZ-DCV**, **DPPZ-IO,** and **DPPZ-IOO** in both conformations. For *s-cis* conformations of **DPPZ-IDO**, **DPPZ-ID,** and **DPPZ-IDD,** insertion of sterically demanding dicyanovinyl groups into indan(di)one twists a molecule mainly around the methine single bond with dihedral angles of φ_1 = 6°, 13°, and 20°, respectively. Theoretically, the exocyclic methine bonds of **DPPZ-IH** without an electron acceptor considerably alternate, that is, bond lengths *c* and *d* are 1.468 Å and 1.334 Å (Table 1). **DPPZ-IO** with the weakest acceptor has the shorter single bond (1.453 Å) and the longer double bond (1.341 Å) than **DPPZ-IH**. This trend continues with the rising strength of the acceptor; for example, for **DPPZ-IDO,** these bond lengths are 1.433 Å and 1.369 Å.

We compared the molecular structures of **DPPZ-EWG**, obtained from crystals, with DFT-optimized structures to reveal the effect of intermolecular interactions on structural parameters (Figure 2). In crystal structures of **DPPZ-IO** and both polymorphs of **DPPZ-DCV**, **DPPZ-ID,** and **DPPZ-IDO**, the *s-cis* conformers were observed in accordance with the calculation. The only exception was found in prismatic crystals of **DPPZ-IOO**, which was ascribed to the blocking of a position of IOO by $CHCl_3$, fixed through a C—H···O═C interaction instead of a CH−π interaction for side phenyls C and D. Intermolecular interactions led to significant deviations from the calculated structure in dihedral angles around the side-phenyl groups and the methine double bond (φ_2). For instance, in the most distorted **DPPZ-IDO**, both side phenyls C and D were rotated only about 75° from dihydrophenazine plane, and the twists around *both* methine exocyclic bonds (φ_1 and φ_2) were close to 20°. Such a huge twist around the formally double bond in a neutral form relates well with the evolution of bond lengths, when going from weaker to stronger acceptors (Table 1). The experimental bond lengths *c* and *d* semi-quantitatively agree with calculations, being 1.453(2)

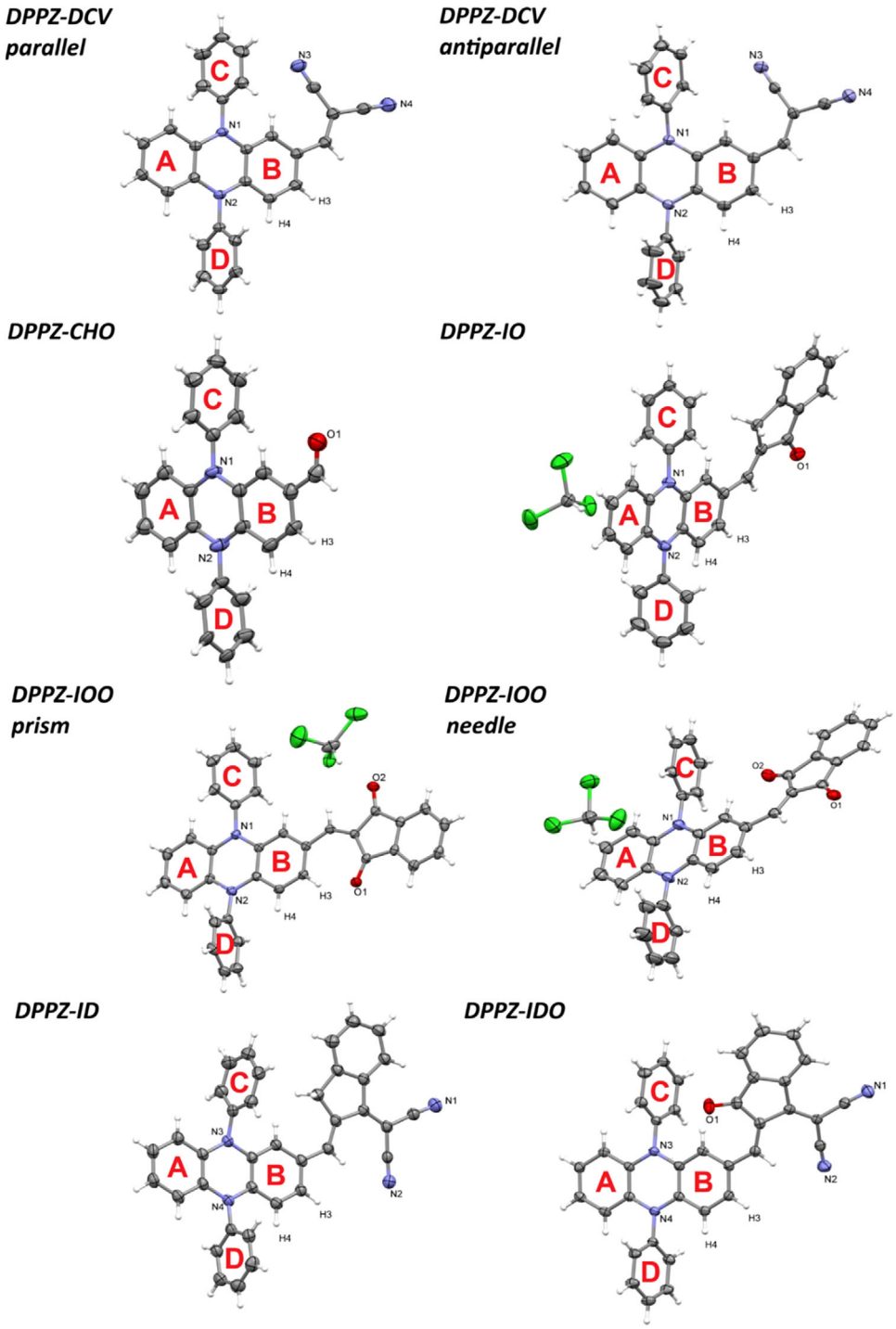

Figure 2. Molecular structures of **DPPZ-EWG** in ORTEP view, drawn at the 50% probability level.

Å and 1.344(2) Å for **DPPZ-IO** and 1.428(2) Å and 1.376(2) Å for **DPPZ-IDO**. Furthermore, the bond lengths *a* between *para* nitrogen atoms and styryl bridges were considerably shortened from 1.398(2) Å (**DPPZ-IO**) to 1.380(2) Å (**DPPZ-IDO**) with increasing acceptor strength. Therefore, these trends in BLA apparently indicate the increasing weight of zwitterionic resonance form in the electronic structure both in solution and crystal states (Figure 1Bc). Nevertheless, all compounds fall into the polyene-like interval, not the betaine-like one.[18b] The cyanine limit with bond length equalization has equal contribution of both neutral and zwitterionic forms and is usually achieved for merocyanines with either a pure polymethine-type bridge[34,36] or five-membered heterocycles.[18b,37] The aromaticity of a benzene ring in the styryl bridge probably suppresses overcoming the cyanine limit leading to quinoidization even for a combination of a strong donor and a strong acceptor.

Specific nearest-neighbor intermolecular interactions in molecular packing were highlighted (Figure 3). Especially,

Table 1. Structural parameters of **DPPZ-EWG** in optimized structure (DFT: CAM-B3LYP/6-311G(d,p) with $CHCl_3$ involved through PCM) and crystal structure.

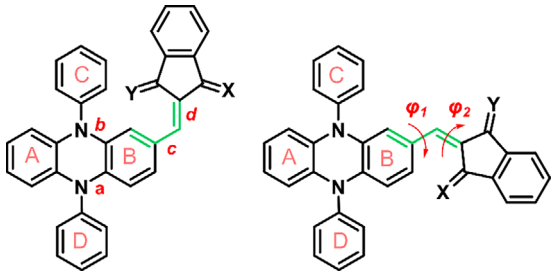

DPPZ-EWG		ΔE_{ct}[a]	φ_1[b] Exp	φ_2[b] Exp	a[c] Theor	a[c] Exp	b[c] Theor	b[c] Exp	c[c] Theor	c[c] Exp	d[c] Theor	d[c] Exp
IH[d]	*cis*	0.146			1.403		1.406		1.468		1.334	
	trans				1.403		1.405		1.469		1.333	
IO	*cis*	0.535	11.08	−1.27	1.394	1.398(2)	1.404	1.405(2)	1.453	1.453(2)	1.341	1.344(3)
	trans				1.395		1.404		1.454		1.340	
IOO	*cis*	0.290			1.384		1.405		1.437		1.356	
	trans		177.65	−179.30	1.385	1.382(2)	1.404	1.409(2)	1.437	1.433(2)	1.357	1.365(2)
ID	*cis*	0.499	5.52	1.97	1.389	1.384(3)	1.403	1.406(3)	1.449	1.443(4)	1.352	1.357(4)
	trans				1.390		1.402		1.451		1.350	
IDO	*cis*	0.304	18.92	25.76	1.378	1.380(2)	1.404	1.409(2)	1.433	1.428(2)	1.369	1.376(2)
	trans				1.379		1.404		1.433		1.368	
IDD	*cis*	1.122			1.380		1.400		1.436		1.364	
	trans				1.383		1.400		1.442		1.360	

[a] Energy difference between s-cis (left) and s-trans (right) conformers [kcal·mol^{-1}].
[b] Dihedral angles [°].
[c] Selected bond lengths [Å].
[d] Hypothetical indan compound with X = Y = H_2.

π-stacking motifs are at the center of our interest, as they considerably affect the photophysical properties in solid state.[29,38] Except for **DPPZ-CHO**, all compounds formed π-stacked dimeric structures in the crystal packing. **DPPZ-IOO** (needle crystals) formed nearly the same type of π-stacking as **DPPZ-IO**. The packing of the rest of the compounds is shown in Figure 3. As for other reported monomethine merocyanines, the most important packing motif is the formation of columns with alternating dimers in an antiparallel arrangement.[39] The only exception within our set was the new polymorph of **DPPZ-DCV**. The infinite columns with parallel arrangement of the molecules were formed by the π-π stacks with an overlap between B and A of adjacent molecules and were interconnected with adjacent columns by CH–π interaction between side phenyls D and unsubstituted phenazine benzene rings A. In the antiparallel polymorph of **DPPZ-DCV**, molecules in the π-π stacked dimer interacted through a wider overlap of DCV vinyl with unsubstituted A rings of dihydrophenazine with an interplane distance of 3.929 Å. In addition, another molecule stacked with the B ring of dihydrophenazine with narrower overlap and closer interplane distance (3.300 Å). Close (proximal) π-π stacks in **DPPZ-IO** and **DPPZ-IOO** solvates were formed through an overlap between the indan(di)one benzene ring with one of the phenazine rings, while distant (distal) dimers were formed by a mutual indan(di)one overlap. Both closer and distant dimers of **DPPZ-ID** were formed by similar interactions between DCV and either unsubstituted benzene ring A or substituted benzene ring B of dihydrophenazine, respectively, as in the antiparallel polymorph of **DPPZ-DCV**. In **DPPZ-IDO,** both alternating π-π stacked dimers arose from an overlap of acceptor parts, either in a benzene-vinylene (closer) or benzene-benzene (distant) fashion. Such dimers with specific π-stacking are critical because they significantly impact exciton coupling and related photophysical properties.

Electrochemical measurements of **DPPZ-EWG** were carried out primarily using CV and RDEV to investigate the trend of electron donating and accepting strength. The cyclic voltammograms of **DPPZ-EWG** derivatives showed one-electron irreversible reduction process and two reversible oxidation processes (Figures 4 and S2). These results imply stability of radical cation and dication species and instability of radical anions.[23] The first half-wave redox potentials from RDEV and estimated HOMO and LUMO energy levels are summarized in Table S8, together with the results of DFT calculations based on the energy differences between adiabatic neutral species in the singlet ground state and charged radical ions in the doublet state involving the solvent effect of acetonitrile.[40,41] The first and second oxidation potentials of **DPPZ-EWG** with indan(di)one acceptors were negatively shifted compared to **DPPZ-CHO** and **DPPZ-DCV,** probably due to the extended conjugation, even

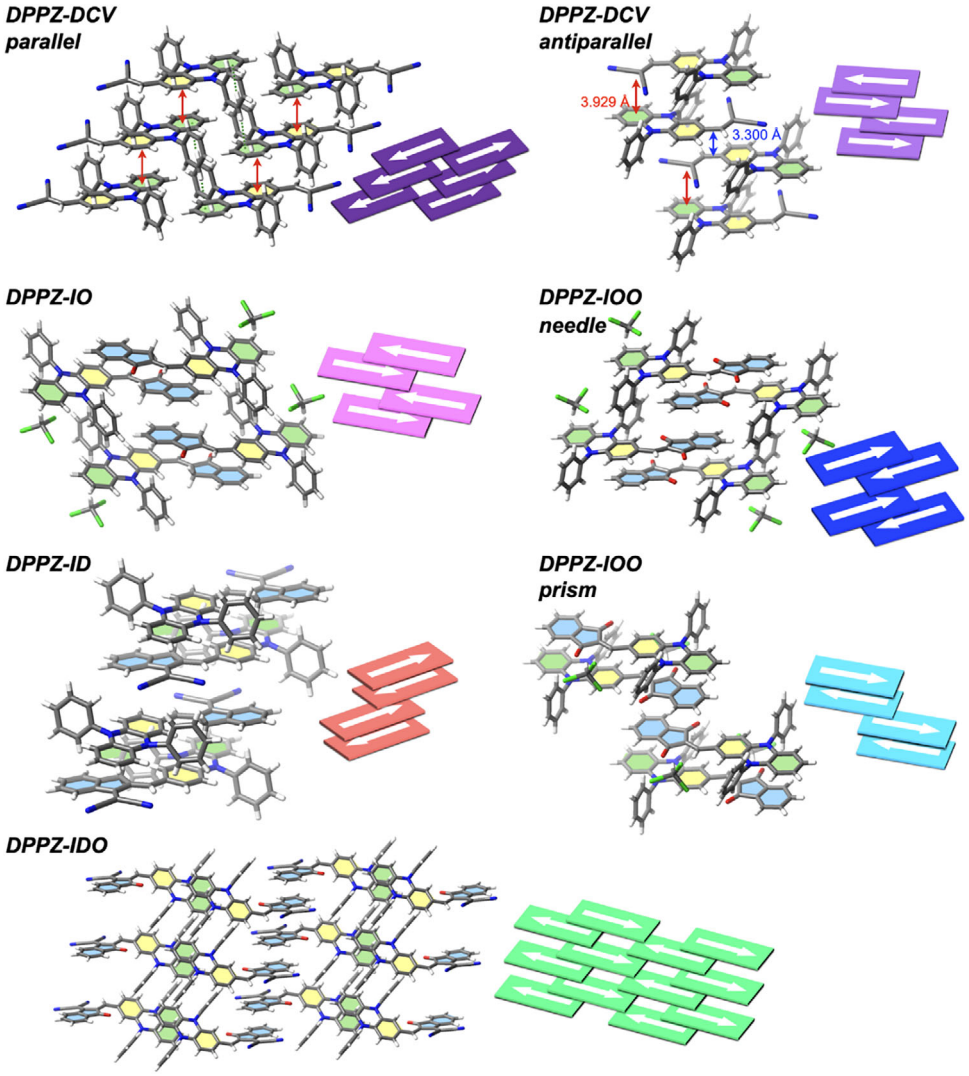

Figure 3. Columnar arrangement of **DPPZ-EWG** with alternating close and distant dimers. For **DPPZ-DCV** (parallel), highly disordered solvent ($CHCl_3$) density was removed by the SQUEEZE program.

though stronger electron acceptor groups were introduced. On the contrary, lower reduction potentials are presumably dominated by the intrinsic electron-accepting ability of acceptor units. These experimental results agree well with the estimation from DFT calculations. Results show the marginal differences in HOMO energy within the set and dramatic differences in LUMO energies, for example, more than 1 eV between **DPPZ-IO** and **DPPZ-IDD**. **DPPZ-ID**, **DPPZ-IDO**, and **DPPZ-IDD** show ultranarrow electrochemical gap (Figure 5). Not surprisingly, spin densities of radical cation and anion are mainly localized on dihydrophenazine donor and indan(di)one acceptor, respectively (Figure 6).

The main task of the molecular design, that is, tuning absorption and emission bands toward the infrared region through the strength of an acceptor, was accomplished. In Figure 7A, the absorption spectra in chloroform followed the trend of a bathochromic shift with decreasing LUMO energy and achieved the NIR region for **DPPZ-ID** (695 nm), **DPPZ-IDO** (778 nm), and **DPPZ-IDD** (880 nm). These absorption maxima of **DPPZ-EWG** were significantly bathochromically shifted compared to their analogues with triphenylamine or carbazole donors in dichloromethane.[20,30a] Especially, the bathochromic shift of **DPPZ-IDD** reached up to 240 nm by introducing *meta*-nitrogen atom. PMMA film of these compounds showed a similar trend with respect to the acceptor strength (Figure S8), but they are always slightly blue shifted with respect to the $CHCl_3$ solutions. Absorption of amorphous thin films showed further bathochromic shift (Figure 7B). Their longest wavelength onsets implied narrow band gaps for **DPPZ-IOO** (1.51 eV) and **DPPZ-ID** (1.30 eV) and even ultranarrow optical band gaps for **DPPZ-IDO** (1.16 eV) and **DPPZ-IDD** (1.09 eV). The exact values of all absorption maxima are summarized in Table S10. In addition to this straightforward dependence of the absorption maxima on the acceptor strength, several other optical properties require further discussion. These include the nature of the electronic transitions between the ground and excited states, the vibronic structure of the spectra, solvatofluorochromism, fluorescence intensity, and the emission behavior in thin films and crystals.

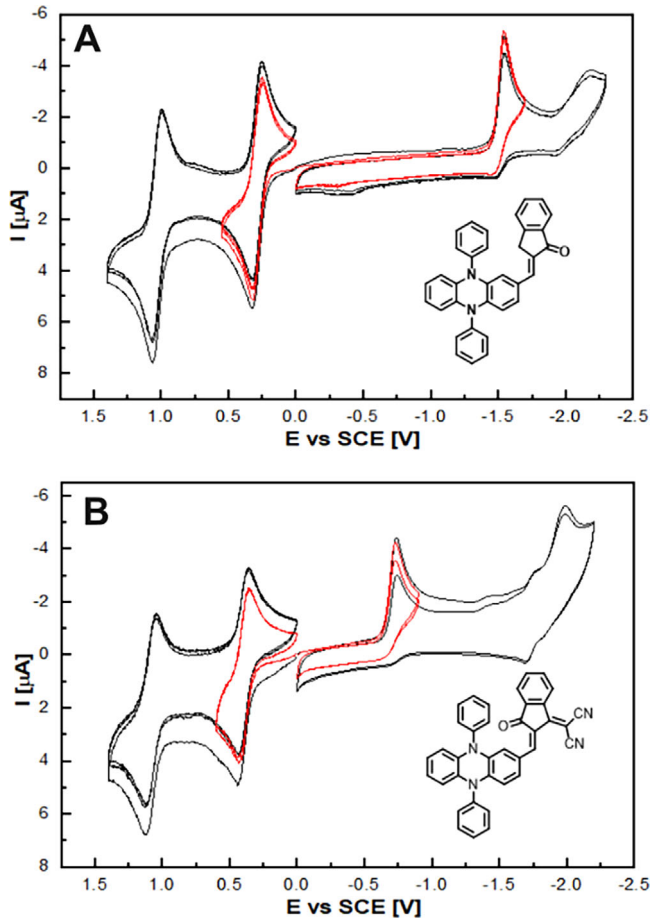

Figure 4. Representative cyclic voltammograms of A) **DPPZ-IO** and B) **DPPZ-IDO** measured in CH_3CN with 0.1 M Bu_4NPF_6. at the scan rate of 100 mV/s.

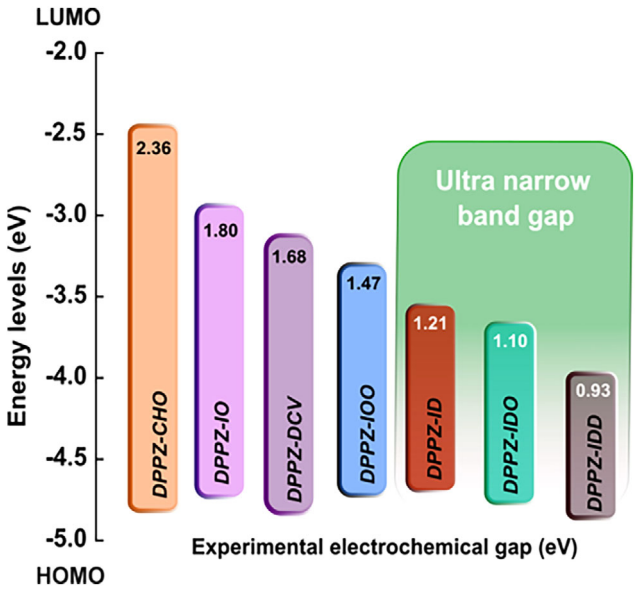

Figure 5. Graphical presentation of HOMO and LUMO energies and electrochemical gaps of **DPPZ-EWG**.

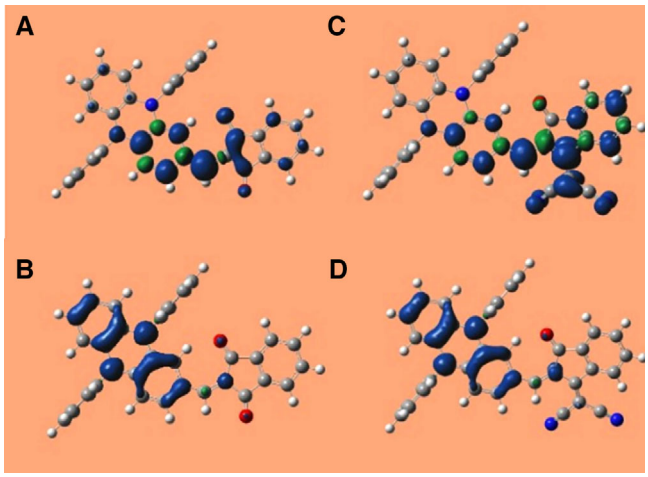

Figure 6. SCF spin densities of the A) C) radical anion and B) D) radical cation of **DPPZ-IOO** (left) and **DPPZ-IDO** (right) calculated at the UB3LYP/6-311G(d,p). Isovalue = 0.002.

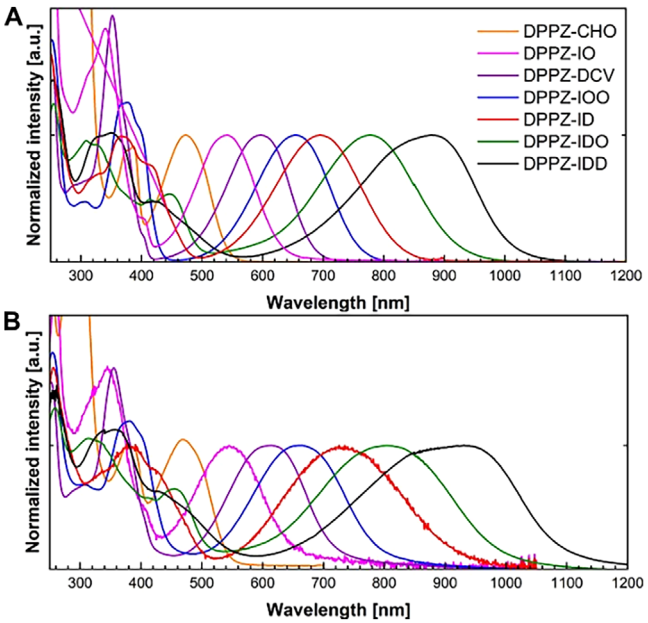

Figure 7. Absorption spectra of **DPPZ-EWG** in A) $CHCl_3$ solution and B) neat film.

The character of the electronic transitions in Vis-NIR regions was studied using TD DFT calculation with both B3LYP and CAM-B3LYP[42] xc functionals (see Table 2 and S6 in Supporting Information). B3LYP excitation energies of $S_0 \rightarrow S_1$ transition of *s-cis* conformations are close to the experimental longest absorption maxima and enable the interpretation of the whole absorption spectrum, as shown in Figure 8 for **DPPZ-IDO** as an example. The absorption bands in Vis–NIR regions attribute to mainly three transitions of $S_0 \rightarrow S_n$ (n = 1–3), each well defined by a dominant monoexcited configuration HOMO→LUMO, HOMO→LUMO+1, and HOMO–1→LUMO, respectively. The first transition of **DPPZ-IDO**, named CT_1, is the same for all other compounds except **DPPZ-IDD** calculated by B3LYP (Table 2). The $S_0 \rightarrow S_3$ transition of **DPPZ-IDO**, named CT_2, relates to $S_0 \rightarrow S_2$ of **DPPZ-ID** (Figure S4).

Table 2. Summary of electronic transitions of **DPPZ-EWG** with *s-cis* conformations calculated with TD DFT at the B3LYP and CAM-B3LYP/6-311G(d,p) with PCM ($CHCl_3$).

	B3LYP						CAM-B3LYP						Exp.
	$S_0 \rightarrow S_1$		$S_0 \rightarrow S_2$		$S_0 \rightarrow S_3$		$S_0 \rightarrow S_1$		$S_0 \rightarrow S_2$		$S_0 \rightarrow S_3$		$S_0 \rightarrow S_1$
Compounds	E [eV]	f_{osc} [a]	E [eV]	f_{osc} [a]	E [eV]	f_{osc} [a]	E [eV]	f_{osc} [a]	E [eV]	f_{osc} [a]	E [eV]	f_{osc} [a]	E [eV] [b]
DPPZ-CHO	2.56	0.12	3.27	0.08	3.28	0.00	3.07	0.13	3.86	0.19	4.2	0.00	2.62
DPPZ-IO	2.12	0.40	3.11	0.05	3.18	0.00	2.84	0.48	3.70	0.29	3.72	0.00	2.29
DPPZ-DCV	2.05	0.34	3.25	0.00	3.4	0.00	2.53	0.45	3.73	0.08	3.99	0.82	2.08
DPPZ-IOO	1.90	0.44	2.34	0.01	3.15	0.00	2.46	0.56	3.57	0.01	3.62	0.00	1.89
DPPZ-ID	1.66	0.55	2.87	0.49	3.04	0.06	2.32	0.68	3.49	0.42	3.61	0.02	1.78
DPPZ-IDO	1.60	0.45	1.98	0.10	2.83	0.48	2.17	0.71	2.96	0.02	3.46	0.52	1.59
DPPZ-IDD	1.44	0.03	1.58	0.50	2.60	0.18	1.99	0.49	2.38	0.11	3.23	0.16	1.41

[a] Oscillator strength.
[b] The longest absorption maximum in $CHCl_3$ solution.

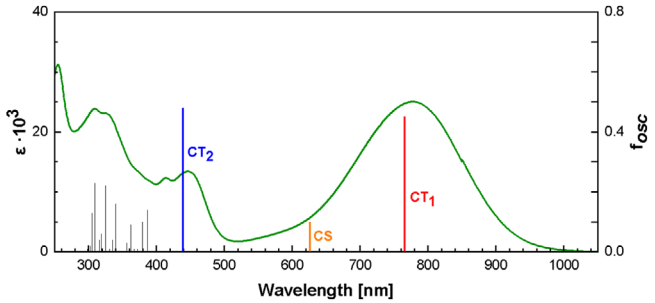

Figure 8. The experimental absorption spectrum of **DPPZ-IDO** in $CHCl_3$ and calculated excitation energy bars computed using *s-cis* geometry with TD DFT at the B3LYP/6-311G(d,p) with PCM ($CHCl_3$). The characters of charge-transfer (CT) and charge-separation (CS) transitions are demonstrated in Figure 9.

Both CT_1 and CT_2 transitions show nearly the same "particle" natural transition orbitals (NTOs) delocalized on methine and acceptor moieties and similar "hole" NTOs mainly delocalized on dihydrophenazine with a bit different molecular orbital shape between HOMO and HOMO–1 (Figure 9). The crucial characteristics of both these charge transfer transitions is a more effective depletion of an electron density from *meta* nitrogen atom, as compared to *para* nitrogen, which is typical for simple *meta* chromophores, as compared to regioisomeric *para* chromophores.[43] Thus, the transition to the S_1 state is going on pre-polarized electronic structure with the effect of *para* nitrogen donor in the ground state in contrast to conventional *meta* chromophores. Not surprisingly, the energies of CT_1 and CT_2 transitions of **DPPZ-IDO** are closer to **DPPZ-ID** than to **DPPZ-IOO** (Figures 7, 8, and S4), as the local DCV group is a considerably stronger acceptor than carbonyl in complex IDO acceptor (Figure 9). Altogether, considering two nitrogen atoms and two acceptor terminals separately is crucial to understand these two CT transitions. On the other hand, the $S_0 \rightarrow S_2$ transition of **DPPZ-IDO**, named CS, is significantly different from CT transitions and re lates to $S_0 \rightarrow S_2$ of **DPPZ-IOO** (Figure S4). It can be characterized as an enhanced electron transfer from dihydrophenazine donor to an indan(di)one acceptor, leading to partial (**DPPZ-IDO** on Figure 9) or even full (**DPPZ-IOO** on Figure S4a) charge separation. On the contrary to both CT states, the CS one shows a tendency to adopt an *ortho*-quinodimethane-like electronic structure on indan(di)one benzene ring in the S_2 state. While CT_1 and CT_2 transitions can be easily detected as the distinct bands with moderate oscillator strengths (f_{osc}) in the absorption spectrum, CS transition is too weak due to small f_{osc} and manifests itself only as a shoulder on short-wavelength region of CT_1 band (Figure 8). Superposition of an intense CT_1 band at a shorter wavelength and a weaker CS band at a longer wavelength would cause an asymmetrical shape of the longest absorption band of DPPZ-IDD at 880 nm compared to all other compounds (Figure 7).

While the absorption spectra in chloroform are blurred (Figure 7A), well-structured absorption bands with vibronic pattern can be observed in cyclohexane (Figure 10). The wavenumber differences between 0–0 and 0–1 vibronic bands in **DPPZ-IOO** and **DPPZ-DCV** were around 1200 cm^{-1}, which corresponds well with the C—C bond stretching vibrations of merocyanines.[44] Except for a twisted **DPPZ-IDD**, there is a clear relation between the decreasing excitation energy (given by an acceptor strength) and the raising ratio of 0–0 and 0–1 vibronic band intensity. The closer the merocyanines are in polyene-like region to the cyanine limit, the more suppressed is the relative intensity of 0–1 transition.[12a,45] Therefore, the evolution of a vibronic structure in Figure 10A is a spectral manifestation of the trend, estimated from BLA (Table 1). Even in weakly polar toluene solution, the absorption spectra of all compounds showed broad bands without vibronic structure (Figure S7). While **DPPZ-IO** and **DPPZ-ID** showed positive solvatochromism, **DPPZ-IOO**, **DPPZ-IDO,** and **DPPZ-IDD** showed inverse solvatochromism, that is, positive up to chloroform and then negative toward acetonitrile (Figure 11 for **DPPZ-IOO** and Table S10). Inverse solvatochromism often implies electronic structure near the cyanine limit,[34] but that was not observed in the more polar **DPPZ-ID** than **DPPZ-IOO**. Furthermore, this inverse solvatochromism led to broadened absorption bands without characteristic evolution, suppressing a 0–1 relative intensity.[35] We speculate that the small bathochromic shift of all three indandione derivatives in

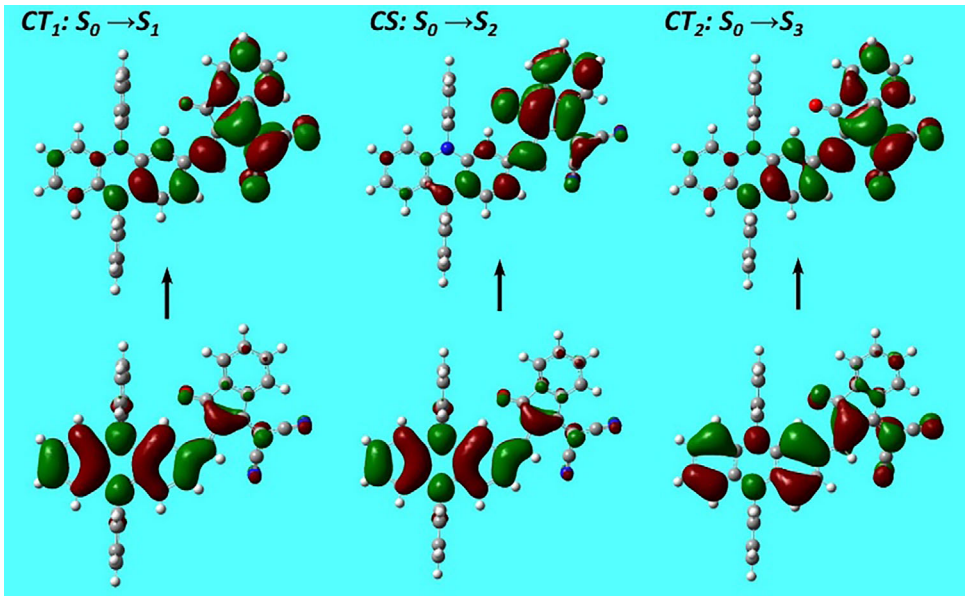

Figure 9. Hole and particle pairs of NTOs of **DPPZ-IDO** for $S_0 \rightarrow S_1$ (HOMO→LUMO), $S_0 \rightarrow S_2$ (HOMO→LUMO+1), and $S_0 \rightarrow S_3$ (HOMO−1→LUMO) transitions, calculated with TD DFT at the B3LYP/6-31G(d,p) with PCM ($CHCl_3$), isovalue 0.02.

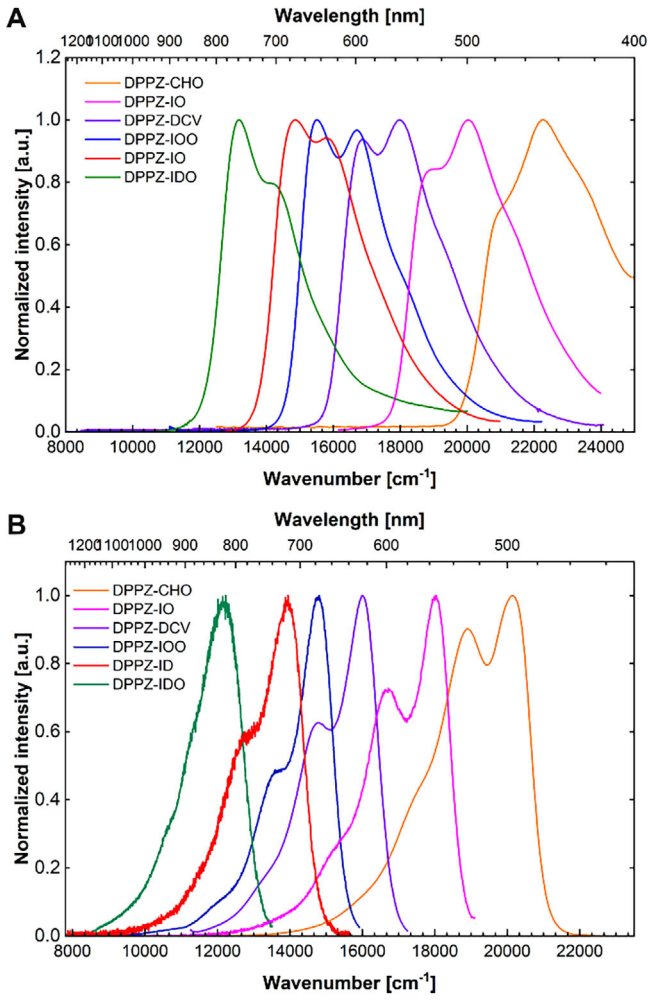

Figure 10. A) Absorption and B) fluorescence spectra of **DPPZ-EWG** except **DPPZ-IDD** in cyclohexane.

Table 3. Calculated bond lengths *a*—*d* [Å] in the S_0 and S_1 states (DFT: CAM-B3LYP/6-311G(d,p) with cyclohexane involved through PCM).

Compounds	States	*a*	*b*	*c*	*d*
DPPZ-IO	S_0	1.395	1.405	1.454	1.340
	S_1	1.390	1.389	1.422	1.369
DPPZ-IOO	S_0	1.386	1.405	1.438	1.355
	S_1	1.396	1.390	1.419	1.386
DPPZ-ID	S_0	1.391	1.404	1.450	1.351
	S_1	1.388	1.391	1.430	1.379
DPPZ-IDO	S_0	1.380	1.405	1.435	1.368
	S_1	1.393	1.390	1.428	1.392

halogenated solvents may be caused either by an increased population of *s-trans* conformers by specific intermolecular interactions with solvents, as observed in crystal structure, or the role of the higher refractive index.

Fluorescence spectra and photoluminescence quantum yields (PLQY) of **DPPZ-EWG** derivatives depended strongly both on structure and environment (Table S10 and Figure S7). The simplest situation was found for fluorescence in nonpolar cyclohexane (Figure 10B). Except for **DPPZ-IDD** with a very low signal-to-noise ratio (Figure S9), all compounds showed well-resolved fluorescence bands from visible (493 nm for **DPPZ-CHO**) to NIR regions (832 nm for **DPPZ-IDO**) following the same sequence as their absorption maxima. The vibronic structure with about a 1200 cm^{-1} interval consistently showed a 0–0 absolute maximum and gradual suppression of 0–1 relative intensity (Figure 10B). As the prominent vibronic pattern relates to C—C bond stretching, the vibronic relaxation in the excited state mainly causes a dramatic extension of *d* bond and shortening of exocyclic *c* bond according to the geometry optimization in the S_1 state (Table 3). During relaxation from the Franck-Condon

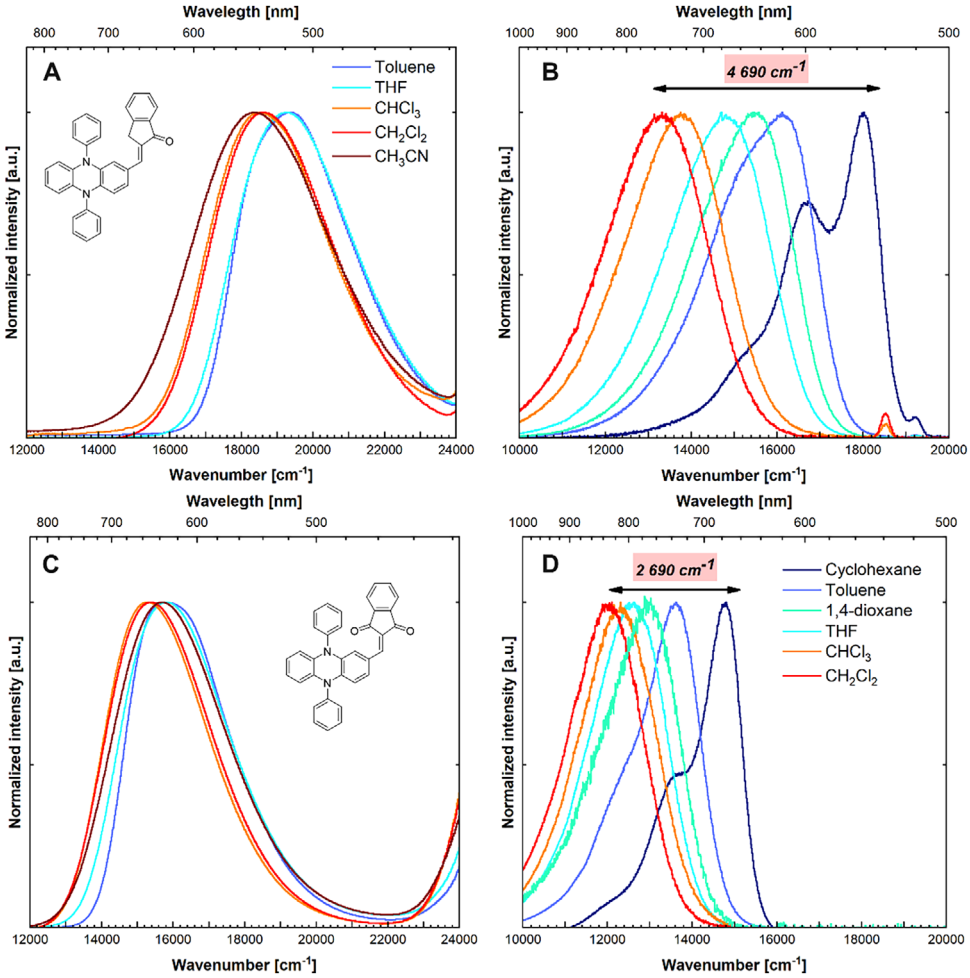

Figure 11. Solvatochromism (left) and solvatofluorochromism (right) of A) B) **DPPZ-IO** and C) D) **DPPZ-IOO**.

state with S_0 geometry to relaxed S_1 geometry, while the differences in *d* bond length $\Delta d(S_1-S_0)$ of **DPPZ-IO**, **DPPZ-IOO**, **DPPZ-ID,** and **DPPZ-IDO** are relatively comparable (+0.029, +0.031, +0.028, and +0.024 Å, respectively), the corresponding $\Delta c(S_1-S_0)$ values depend dramatically on an acceptor strength (−0.032, −0.019, −0.020, and −0.007 Å, respectively). These tendencies are consequently responsible for the decrease of the relative intensity of 0–1 vibronic band, relating to stretching of *c* bond according to the Frank-Condon principle.[46] We note only a considerable shortening of *b* bonds, which are consistent with a CT excitation originating mainly from *meta*-nitrogen atoms. The shapes of both the absorption and fluorescence bands in cyclohexane imply that the larger is a zwitterionic character in the S_0 state; that is, the larger the proximity of a compound to a cyanine limit, the lower the difference between S_0 and S_1 hypersurface minima with respect to prominent *c* bond length coordinate and, consequently, the lower is the structural relaxation energy upon excitation.

All compounds without any exception showed positive solvatofluorochromism (Figure 11 and S7). The vibronic structures of fluorescence spectra were poorly resolved even in weakly polar toluene solution and completely disappeared with raising polarity of the solvent, due to the inhomogeneous broadening.[47] Sufficiently strong fluorescence intensities for PLQY measurements were found only in a few cases (Table S10). In toluene solutions, raising acceptor strength clearly decreased PLQYs from **DPPZ-CHO** (60.0%) over **DPPZ-IO** (28.7%) to **DPPZ-DCV** (9.0%) and **DPPZ-IOO** (3.0%). A further decrease of PLQY was observed in polar solvents; for example, in chloroform for **DPPZ-CHO** (3.0%), **DPPZ-DCV** (2.2%), and **DPPZ-IOO** (0.3%). But the dependence of solvatofluorochromism on the molecular structure was not as straightforward as, for instance, for PLQY. For nearly isomorphic **DPPZ-IO**, **DPPZ-IOO**, **DPPZ-ID,** and **DPPZ-IDO**, the differences between fluorescence maxima in nonpolar cyclohexane and moderately polar dichloromethane (often considered as twice the solvation energy[48]) were 4690, 2690, 3570, and ∼1680 cm^{-1} respectively. We leave open the question of to what extent solvatofluorochromism, that is, energies of fluorescence maxima in each solvent, is driven by intramolecular structural relaxation (dominant in nonpolar cyclohexane) and intermolecular solute–solvent, mainly dipole–dipole, interactions.

Monomethine merocyanines are well known to undergo fluorescence quenching via twisting in the S_1 state toward a conical intersection, followed by a hot back-twist to the ground state minimum.[18b] Such twisted intramolecular charge transfer (TICT) of merocyanine often occurs around a single bond in neutral form or around the double bond in zwitterionic form.[49] As expected from TD DFT calculations,[50] B3LYP, and CAM-B3LYP xc

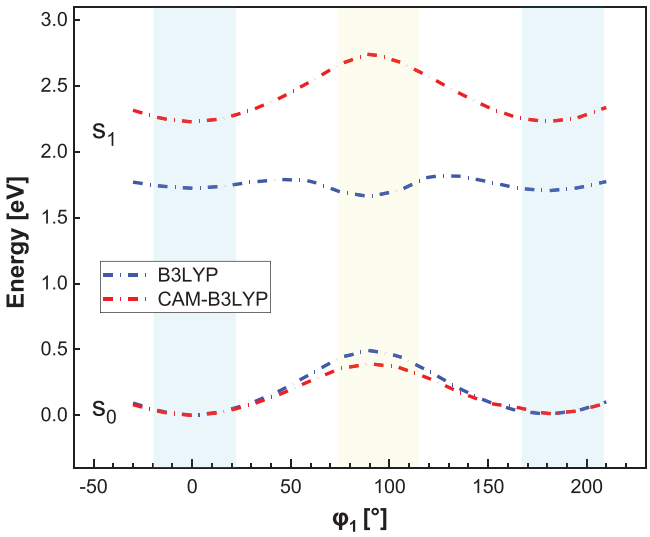

Figure 12. Energy dependence on the twist angle of **DPPZ-IOO** in the ground and excited states, calculated at the B3LYP and CAM-B3LYP/6-311G(d,p) with PCM ($CHCl_3$).

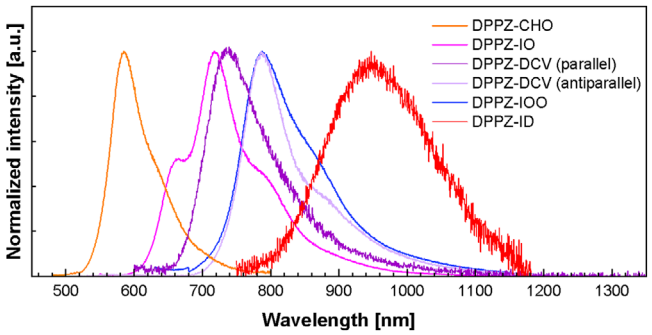

Figure 13. Fluorescence spectra of **DPPZ-EWG** in polycrystalline states.

functionals show a dramatic difference in the dependence of an optimized S_1 state energy on the twist angle φ_1, as shown for **DPPZ-IOO** as an example (Figure 12, and see detailed analysis in S6 Supporting Information). Regardless of the different solvent effect models, the results revealed similarities with a benchmark study about the simpler DA compounds.[50b] The energy profiles for the S_1 state computed with B3LYP and CAM-B3LYP begin to diverge significantly at $\varphi_1 \approx 45°$. While B3LYP suggests the TICT state as a global minimum and planar intramolecular charge transfer ($PICT_c$ and $PICT_t$) states as local minima, CAM-B3LYP converged to $PICT_c$ and $PICT_t$ states with rotational barriers in the excited state. And B3LYP computed transition energies relating the fluorescence at the planar geometry ($PICT_t$) are closer to the experimental fluorescence energies (Table S9). As CAM-B3LYP showed similar trends as more sophisticated QCH methods, including EOM-CCSD[50a] and LCC2,[50b] we conclude that the weak fluorescence observed for the four compounds in polar solvents in Figure 12 originates from planar geometries in the S_1 state mainly, and the twist geometry leading to the nonradiative deactivation is limited within the small twist angles region and prevents the TICT geometry with full charge separation.[51]

Solid-state fluorescence of polycrystalline powders was detected for all compounds except **DPPZ-IDD** (Figure 13), while an emission of **DPPZ-IDO** around 1100 nm was extremely weak with a low signal-to-noise ratio (Figure S9). Among these emissive derivatives, similar trends in fluorescence wavelength were found between the solution and the amorphous films (Figure S8). Neat film's SSF is generally red shifted with respect to PMMA films (Table S10). Powder X-ray diffraction of the emissive polycrystalline samples suggested a similar packing structure with single crystals except for **DPPZ-IOO** (Figure S10). The neat film of **DPPZ-DCV** showed a fluorescence maximum at 761 nm, while PMMA films exhibited maximum at a 706 nm, which is comparable to the reported nanoparticles (700 nm).[27] This significant red shift of neat film is presumably due to the intermolecular interaction with surrounding adjacent molecules with random arrangement. The SSF maximum of the antiparallel arranged polymorph was observed at a longer wavelength of 785 nm than that of the parallel one at 731 nm, which we attribute to the 0–1 vibronic maximum of the former and the 0–0 maximum of the latter.[52] As an antiparallel arrangement generally prevails for all compounds according to single-crystal XRD (Figure 3), 0–1 vibronic maximum may be quite common, but without a doubt it is observed only for **DPPZ-IO** (Figure 13). Weak solid-state emission with structureless symmetrical bands of **DPPZ-ID** (975 nm) and **DPPZ-IDO** (~1100 nm) is tentatively attributed to excimer emission from isolated π-stacked dimers (Figure 3).[29a] PLQYs of polycrystalline samples are typically too low to quantify, as an aggregation accelerates fluorescence quenching processes, including dissipation of excitation energy through energy transfer and nonradiative decay.[53] Nevertheless, a considerable increase in PLQY of **DPPZ-IO** upon solidification was observed from $CHCl_3$ solution (PLQY <<1%) to crystal (PLQY = 4.0%) and doped PMMA film (PLQY = 8.4%). Similar but less pronounced enhancements were seen for **DPPZ-IOO** (0.3% in $CHCl_3$ and 1.1% both in powder and PMMA film). Such an enhancement of PLQY in the solid state may imply suppression of twist and rotational motions leading to nonradiative decay in the solution state.[54]

We note only that all **DPPZ-EWG** derivatives were sufficiently stable with respect to the above-mentioned experiments, especially in the solid state under visible light. We have observed two types of reactivity. First, upon irradiation by UV radiation in solution, the compounds degraded with color changes (Figures S11, S12). We ascribe this to the photooxidation in higher excited states (Figure S13).[26]. Second, compounds with low-lying LUMO, like **DPPZ-IDO** and **DPPZ-IDD**, show irregular changes of absorption in polar solvents with high donor numbers (DMSO, methanol, pyridine). Thus, these solvents were excluded from solvatochromism and solvatofluorochromism studies.

3. Experimental

3.1. Synthesis and Characterization

3.1.1. DPPZ-CHO

In a 250 mL round-bottomed flask, 5,10-diphenyldihydrophenazine (**DPPZ**, 2.00 g, 5.98 mmol, 1.00 eq.) was suspended in anhydrous

DMF (100 mL) and cooled to 0 °C with an ice bath. After adding $POCl_3$ (1.12 mL, 11.9 mmol, 2.00 eq.) dropwise, the resulting mixture was heated to 60 °C and stirred for 3 hours under a nitrogen atmosphere. After cooling down to room temperature, the mixture was poured on ice, followed by precipitation of an orange solid. Crude product was purified by column chromatography (mobile phase chloroform/*n*-hexane 1/4) and crystallized from a mixture of ethyl acetate and *n*-hexane. It was obtained 1.47 g of **DPPZ-CHO** as orange crystals (63%).

R_f: 0.22 (*n*-hexane/EtOAc = 7/1, *v/v*), **m.p**. 239.5–240.0 °C. **^{1}H NMR** (400 MHz, C_6D_6): δ 9.29 (s, 1H), 7.14–7.07 (m, 6H), 7.05–6.97 (m, 4H), 6.54 (d, J = 9.2 Hz, 1H), 6.43 (s, 1H), 6.24–6.21 (m, 1H), 6.19–7.16 (m, 1H), 5.73 (d, J = 7.7 Hz, 1H), 5.69 (d, J = 7.7 Hz, 1H), 5.61 (d, J = 8.1 Hz, 1H). **^{13}C NMR** (101 MHz, C_6D_6): δ 188.9, 142.6, 139.5, 139.4, 137.7, 136.7, 135.5, 131.8, 131.6, 131.3, 130.9, 130.9, 128.7, 128.4, 127.5, 122.9, 121.5, 113.8, 113.4, 111.9, 110.3. **HRMS**: $[M]^+$ Calcd. for $C_{25}H_{18}N_2O$ 362.14136; found 362.14100.

3.1.2. DPPZ-IO

In a 100 mL round-bottomed flask, a mixture of **DPPZ-CHO** (600 mg, 1.65 mmol, 1.00 eq.) and 1-indanone (328 mg, 2.48 mmol, 1.50 eq.) in $CHCl_3$ (50 mL) was treated with 6M NaOH (1.10 mL, 6.60 mmol, 4.00 eq.) and stirred at room temperature for 18 hours. The reaction was quenched by adding water (20 mL). After the aqueous phase was extracted with ethyl acetate (3 × 50 mL). After drying over Na_2SO_4, the organic phase was evaporated under reduced pressure. Crude product was purified by column chromatography (mobile phase $CHCl_3$/*n*-hexane 1/3) and crystallized from a mixture of $CHCl_3$ and *n*-hexane. It was obtained 400 mg of molecule **DPPZ-IO** as purple crystals (51%).

R_f: 0.25 (*n*-hexane/EtOAc = 3/1, *v/v*), **m.p**. 211.4–212.0 °C. **^{1}H NMR** (500 MHz, DMSO-d_6): δ 7.81 (t, J = 7.5 Hz, 2H), 7.73 (t, J = 7.5 Hz, 2H), 7.69–7.61 (m, 3H), 7.58 (t, J = 7.3 Hz, 1H), 7.53 (d, J = 7.5 Hz, 2H), 7.50–7.40 (m, 4H), 6.98 (s, 1H), 6.73 (d, J = 8.1 Hz, 1H), 6.35 (t, J = 7.5 Hz, 1H), 6.30 (t, J = 7.4 Hz, 1H), 5.83 (s, 1H), 5.62–5.61 (m, 1H), 5.54–5.51 (m, 2H), 3.33 (overlap with signal of H_2O in DMSO, 2H). **^{13}C NMR** (126 MHz, DMSO-d_6): δ 192.6, 149.0, 139.0, 138.5, 138.3, 137.6, 136.4, 135.6, 134.9, 134.4, 132.7, 131.9, 131.8, 130.9, 130.5, 129.0, 128.9, 127.7, 127.5, 126.7, 126.2, 123.4, 122.0, 121.0, 112.8, 112.5, 112.4, 111.9, 55.0, 31.7. **HRMS**: $[M]^+$ Calcd. for $C_{34}H_{24}N_2O$ 476.18831; found 476.18887.

3.1.3. DPPZ-DCV

In a 50 mL round-bottomed flask, a mixture of **DPPZ-CHO** (500 mg, 1.38 mmol, 1.00 eq.) and malononitrile (0.230 mL, 4.14 mmol, 3.00 eq.) in CH_2Cl_2 (15 mL) was treated with two drops of piperidine and stirred at room temperature for 20 minutes. The reaction was quenched by adding water (10 mL). After separation, the aqueous phase was extracted with ethyl acetate (3 × 30 mL). After drying over Na_2SO_4, the organic phase was evaporated under reduced pressure. Crude product was purified by column chromatography (mobile phase ethyl acetate/*n*-hexane 1/3) and crystallized from a mixture of ethyl acetate and *n*-hexane. It was obtained 450 mg of **DPPZ-DCV** as purple powder (78%).

R_f: 0.35 (*n*-hexane/EtOAc = 7/1, *v/v*), **m.p**. 219.5–220.0 °C. **^{1}H NMR** (400 MHz, C_6D_6): δ 7.34–7.32 (m, 2H), 7.19–7.18 (m, overlap with C_6D_6 signal, 1H), 7.13–7.08 (m, 4H), 7.05–7.01 (m, 1H), 7.90–6.86 (m, 2H), 6.27 (d, J = 2.1 Hz, 1H), 6.24–6.18 (m, 2H), 6.15 (dt, J = 7.7, 1.5 Hz, 1H), 6.04 (s, 1H), 5.71 (dd, J = 7.8, 1.4 Hz, 1H), 5.63 (dd, J = 7.9, 1.5 Hz, 1H), 5.42 (d, J = 8.5 Hz, 1H). **^{13}C NMR** (101 MHz, C_6D_6): δ 156.0, 143.0, 138.9, 138.6, 137.4, 136.6, 134.7, 132.3, 131.7, 130.7, 130.4, 129.4, 129.2, 129.1, 125.2, 123.6, 121.7, 115.5, 114.3, 114.1, 113.7, 111.8, 111.1, 75.6. **HRMS**: $[M]^+$ Calcd. for $C_{28}H_{18}N_4$ 410.15260; found 410.15337.

3.1.4. DPPZ-IOO

In a 50 mL round-bottomed flask, a mixture of **DPPZ-CHO** (250 mg, 0.689 mmol, 1.00 eq.) and 1,3-indandione (206 mg, 1.38 mmol, 2.00 eq.) in ethanol (20 mL) was treated with two drops of piperidine and refluxed for 18 hours. After cooling down to room temperature, a dark blue solid precipitated in the freezer. After filtration and washing with chilled ethanol, the crude product was purified by column chromatography (mobile phase $CHCl_3$/*n*-hexane 1/4) and recycling HPLC (mobile phase $CHCl_3$). After final crystallization from a mixture of $CHCl_3$ and *n*-hexane, 252 mg of **DPPZ-IOO** was obtained as a dark blue powder (75%).

R_f: 0.29 (*n*-hexane/EtOAc = 3/1, *v/v*), **m.p**. 262.5–263.0 °C. **^{1}H NMR** (400 MHz, C_6D_6): δ 7.68–7.64 (m, 1H), 7.64–7.59 (m, 2H), 7.48–7.45 (m, 2H), 7.39–7.37 (m, 2H), 7.32–7.30 (m, 2H), 7.26–7.24 (m, 1H), 7.13–7.10 (m, 2H), 7.04–7.00 (m, 1H), 6.97–6.89 (m, 4H), 6.25 (dt, J = 7.7, 1.4 Hz, 1H), 6.17 (dt, J = 7.3, 1.4 Hz, 1H), 5.81 (dd, J = 7.9, 1.3 Hz, 1H), 5.68 (dd, J = 7.9, 1.3 Hz, 1H), 5.64 (d, J = 8.6 Hz, 1H). **^{13}C NMR** (101 MHz, C_6D_6): δ 190.3, 189.0, 145.8, 142.9, 142.7, 140.4, 139.8, 139.0, 137.2, 137.0, 135.0, 133.9, 133.9, 133.2, 131.9, 131.6, 131.3, 130.6, 128.8, 128.7, 128.2, 127.9, 125.7, 123.4, 122.6, 121.3, 116.7, 114.2, 113.6, 112.5. **HRMS**: $[M]^+$ Calcd. for $C_{34}H_{22}N_2O_2$ 490.16758; found 490.17148.

3.1.5. DPPZ-ID

In a 100 mL round-bottomed flask, a mixture of **DPPZ-CHO** (600 mg, 1.65 mmol, 1.00 eq.) and **ID** (298 mL, 1.65 mmol, 1.00 eq.) in toluene (50 mL) was treated with two drops of piperidine and refluxed for 18 hours. The reaction was quenched by adding water (20 mL). After separation, the aqueous phase was extracted with ethyl acetate (3 × 30 mL). After drying over Na_2SO_4, the organic phase was evaporated under reduced pressure. Crude product was purified by column chromatography (mobile phase ethyl acetate/*n*-hexane 1/39) and crystallized from a mixture of CH_2Cl_2 and *n*-hexane. It was obtained 738 mg of **DPPZ-ID** as green crystals (73%).

R_f: 0.48 (*n*-hexane/EtOAc = 3/1, *v/v*), **m.p**. 282.5–283.4 °C. **^{1}H NMR** (500 MHz, C_6D_6): δ 8.64 (d, J = 8.1 Hz, 1H), 7.89 (s, 1H), 7.22–7.18 (m, overlap with C_6D_6 signal, 4H), 7.12–7.10 (m, 2H), 7.08–7.05 (m, 4H), 6.99 (t, J = 7.2 Hz, 1H), 6.88 (t, J = 7.6 Hz, 1H), 6.80 (d, J = 7.5 Hz, 1H), 6.32–6.27 (m, 2H), 6.24 (dt, J = 7.6, 1.2 Hz, 1H), 5.84–5.83 (m, 2H), 5.78 (dd, J = 7.8, 1.2 Hz, 1H), 5.61 (d, J = 8.3 Hz, 1H), 2.82 (s, 2H). **^{13}C NMR** (126 MHz, C_6D_6): δ 165.5, 146.7, 140.0, 139.7, 139.3, 137.5, 137.4, 137.0, 136.5, 135.5, 132.9, 132.8, 131.7, 131.6, 131.4, 130.9, 129.0, 128.3, 128.6, 128.3, 127.5, 125.8, 124.6, 122.8, 121.7, 116.4, 116.2, 114.0, 113.3, 113.1, 112.8, 67.6, 37.1. **HRMS**: $[M]^+$ Calcd. for $C_{37}H_{24}N_4$ 524.20010; found 524.20036.

3.1.6. DPPZ-IDO

In a 100 mL round-bottomed flask, a mixture of **DPPZ-CHO** (200 mg, 0.551 mmol, 1.00 eq.) and **IDO** (161 mg, 0.837 mmol, 1.50 eq.) in $CHCl_3$ (20 mL) was treated with two drops of pyridine and refluxed for 18 hours. After cooling to room temperature, solvent was evaporated by reduced pressure. 10 mL of ethanol was added and sonicated for 1 minute. After filtration and washing with chilled ethanol, the crude product was purified by column chromatography (mobile phase $CHCl_3$/*n*-hexane 4/1) and recycling HPLC (mobile phase $CHCl_3$). After final crystallization from a mixture of $CHCl_3$ and *n*-hexane, 217 mg of **DPPZ-IDO** was obtained as a dark green powder (73%).

R_f: 0.31 (*n*-hexane/EtOAc = 3/1, *v/v*), **m.p**. 245.6–246.2 °C. **^{1}H NMR** (400 MHz, C_6D_6): δ 7.41–7.40 (m, 1H), 7.83 (s, 1H), 7.46–7.44 (m, 1H), 7.41–7.37 (m, 2H), 7.32–7.31 (m, 2H), 7.25–7.21 (m, 2H), 7.20–7.19 (m, 1H), 7.14–7.12 (m, 2H), 7.05–7.03 (m, 1H), 6.94–7.92 (m, 2H), 6.85–6.82 (m, 2H), 6.25 (dt, J = 7.6, 1.4 Hz, 1H), 6.16 (td, J = 7.2, 1.8 Hz, 1H), 5.80 (dd, J = 8.0, 1.3 Hz, 1H), 5.70 (dd, J = 7.9, 1.3 Hz, 1H), 5.55 (d, J = 8.4 Hz,

1H). **^{13}C NMR** (126 MHz, C_6D_6): δ 186.5, 162.1,146.0, 144.6, 143.5, 139.9, 139.5, 138.5, 137.7, 137.1, 136.8, 135.0, 134.4, 134.0, 133.2, 132.0, 131.6, 131.2, 130.4, 129.0, 128.9, 125.1, 124.6, 124.0, 123.1, 121.4, 116.5, 115.6, 115.2, 114.6, 113.6, 112.5, 69.4. **HRMS**: $[M]^+$ Calcd. for $C_{37}H_{22}N_4O$ 538.17881; found 538.17963. Minor isomer (not separable): **^{1}H NMR** (400 MHz, C_6D_6) δ 8.20 (d, J = 7.8 Hz, 1H), 7.50–6.77 (overlap with aromatic peaks of major isomer), 6.76 (dd, J = 8.4, 1.4 Hz, 2H), 5.96 (d, J = 2.0 Hz, 1H), 5.89 (s, 1H), 5.73 (d, J = 1.3 Hz, 1H), 5.64 (dd, J = 7.8, 1.3 Hz, 1H), 5.50 (d, J = 8.3 Hz, 1H).

3.1.7. DPPZ-IDD

In a 50 mL two-necked flask, a mixture of **DPPZ-CHO** (150 mg, 0.414 mmol, 1.00 eq.) and **IDD** (120 mg, 0.497 mmol, 1.20 eq.) in acetic anhydride (10 mL) was refluxed under an argon atmosphere for 5 minutes. After cooling down to room temperature, solvent was evaporated under reduced pressure. 10 mL of ethanol was added and sonicated for 1 minute. After filtration and washing with chilled ethanol, the crude product was purified by column chromatography (mobile phase $CHCl_3$/*n*-hexane 1/7) and recycling HPLC (mobile phase $CHCl_3$). After final crystallization from a mixture of $CHCl_3$ and *n*-hexane, 50 mg of **DPPZ-IDD** was obtained as black powder (21%).

R_f: 0.24 (*n*-hexane/EtOAc = 3/1, *v/v*), **m.p**. 240.0 °C decomposed. **^{1}H NMR** (400 MHz, C_6D_6): δ 8.14–8.10 (m, 2H), 8.10 (s, 1H), 7.43 (t, J = 7.7 Hz, 2H), 7.21 (tt, J = 7.6, 1.0 Hz, 1H), 7.11–7.09 (m, 2H), 7.06–7.04 (m, 2H), 7.02–6.98 (m, 1H), 6.79–6.77 (m, 2H), 6.75–6.72 (m, 2H), 6.35 (dd, J = 8.5, 2.0 Hz, 1H), 6.24 (dt, J = 7.6, 1.2 Hz, 1H), 6.15 (dt, J = 7.6, 1.3 Hz, 1H), 5.76 (d, J = 1.3 Hz, 1H), 5.67 (td, J = 8.0, 1.2 Hz, 2H), 5.41 (d, J = 8.4 Hz, 1H). **^{13}C NMR** (101 MHz, C_6D_6): δ 160.0, 143.4, 143.0, 138.0, 137.7, 137.6, 136.4, 133.8, 133.1, 133.0, 131.6, 130.6, 130.0, 123.0, 129.2, 129.1, 125.7, 124.6, 124.3, 121.8, 115.0, 114.9, 114.3, 113.7, 113.4, 110.7, 67.8. **HRMS**: $[M+H]^+$ Calcd. for $C_{40}H_{23}N_6$ 587.1979; found 587.1962 (APCI).

Single-crystal X-ray diffraction: Full sets of diffraction data were collected at 150(2) K with a Bruker D8-Venture diffractometer equipped with Cu (Cu *Kα* radiation; λ = 1.54178 Å) or Mo (Mo *Kα* radiation; λ = 0.71073 Å) microfocus X-ray (IμS) sources, Photon CMOS detector, and Oxford-Cryosystems cooling device. The frames were integrated with the Bruker SAINT software package using a narrow-frame algorithm. Data were corrected for absorption effects using the Multi-Scan method (SADABS). Obtained data are treated by XT-version 2017/1 and SHELXL-2014/7 software implemented in APEX3 v2017.1-0 (Bruker AXS) system.[55] Hydrogen atoms were mostly localized on a different Fourier map; however, to ensure uniformity of treatment of the crystal, all hydrogen atoms were recalculated into idealized positions (riding model) and assigned temperature factors $H_{iso}(H)$ = 1.2 (1.5 for methyl) U_{eq} (pivot atom). H atoms in methyl and vinylidene moieties and hydrogen atoms in aromatic rings were placed with C-H distances of 0.98 and 0.94 Å, respectively.

$R_{int} = \Sigma F_o^2 - F_{o,mean}^2|/\Sigma F_o^2$, $S = [\Sigma(w(F_o^2 - F_c^2)^2)/(N_{diffrs} - N_{params})]^{\frac{1}{2}}$ for all data, $R(F) = \Sigma||F_o| - |F_c|/\Sigma|F_o|$for observed data, $wR(F^2) = [\Sigma(w(F_o^2 - F_c^2)^2)/(\Sigma w(F_o^2)^2)]^{\frac{1}{2}}$ for all data.

Crystallographic data for structural analysis have been deposited with the Cambridge Crystallographic Data Centre, CCDC nos. 2434164–2434170. Copies of this information may be obtained free of charge from The Director, CCDC, 12 Union Road, Cambridge CB2 1EY, UK (fax: +44-1223-336033; e-mail: deposit@ccdc.cam.ac.uk or w w w: http://www.ccdc.cam.ac.uk). The structure of **DPPZ-CHO** is twinned, producing static disorder of all atoms, which was treated by splitting by standard methods into two parts with occupancies of 66:34. Solvent disorders ($CHCl_3$) are treated in **DPPZ-IO** and **DPPZ-IOO** (prism). For **DPPZ-DCV** (parallel), the PLATON/Squeeze program was used to eliminate disordered unassignable solvent ($CHCl_3$) densities.[56]

Powder X-ray diffraction: Powder X-ray diffraction data (Cu *Kα*, λ = 1.5418 Å) of powdered samples were collected on a Diffractometer D8 ADVANCE.DAVINCI (Bruker AXS, Germany) with Bragg-Brentano Θ-Θ goniometer (radius 280 mm) equipped with a LynxEye XE-T detector. The generator was operated at 40 kV and 30 mA. The scan was performed at room temperature from 2 to 50° (*2Θ*) in 0.01° steps with a counting time of 1 second (total step time 192 seconds).

Deposition of thin films: Neat films were prepared by spin coating (1000 rpm for 20 seconds, followed by 2000 rpm for 20 seconds) using 10 mM solution in chloroform on quartz plate. PMMA films were prepared by dissolving 140 mg PMMA an d 2.50 mg of target compounds in 2.60 mL dichloromethane, and spin-coated (1000 rpm for 10 seconds, followed by 2000 rpm for 30 seconds) on quartz plate.

Electrochemical measurements: Electrochemical measurements were carried out in acetonitrile containing 0.1 M Bu_4NPF_6 in a three-electrode cell by CV and RDEV with rotation frequency f = 500 min^{-1}. The scan rate was 100 mV/s. The working electrode was a glassy carbon disk (3 mm in diameter) for CV and RDEV experiments. A saturated calomel electrode (SCE) separated by a bridge filled with supporting electrolyte and Pt wire was used as the reference and auxiliary electrodes. All potentials are given vs. SCE. Voltammetric measurements were performed using a potentiostat PGSTAT 128N (AUTOLAB, Metrohm Autolab B.V., Utrecht, The Netherlands) operated via NOVA 1.11 software.

Absorption and fluorescence: UV-Vis-NIR spectroscopy has been employed for measurements of optical transmittance in the spectral region of 250–1200 nm with a step 0.5 nm by using a JASCO V-770 and a Jasco V-570 spectrometers. Photoluminescence emission spectra were measured by spectrophotometer JASCO FP-8300 in the spectral region of 400–800 nm. Emission in the NIR region was recorded using a Fluorolog-3 spectrophotometer (HORIBA JOVIN IVON INC.) equipped with a Hamamatsu-photonics InGaAs NIR photomultiplier tube detector R5509-43 (550–1300 nm) and a liquid nitrogen cooler C9940. Additionally, an FLS1000 (Edinburgh Instruments) using the Xe lamp (450 W) as an excitation source and a liquid-nitrogen-cooled InGaAs photomultiplier tube as a detector in the spectral region of 400–1350 nm was used. All emission spectra have been corrected to monochromator and detector system response. Photoluminescence quantum yield of samples has been determined by using the integrating sphere coated with $BaSO_4$ on a Quantaurus-QY® C11347(Hamamatsu Photonics) and FLS1000 (Edinburgh Instruments). The reference for liquid samples was quartz cuvettes with pure solvent, and those for solids, $BaSO_4$ powder of spectral quality covered with a quartz lid.

Quantum chemical calculations: Monomer geometries in the ground (neutral, radical cation, and radical anion) and the lowest excited state were optimized by DFT and TD DFT, respectively. B3LYP or CAM-B3LYP[42] XC functionals with 6–311G(d,p) basis sets were used. Vibrational analysis was carried out for all optimized geometries, and only the minima with no imaginary frequency were considered. Solvent effect was introduced by the polarized continuum model (PCM). All calculations were carried out with Gaussian 09 software.[57]

4. Conclusion

The study presents a novel strategy for chromophores exhibiting long-wavelength absorption and NIR fluorescence, that is, streptomerocyanines with dihydrophenazine and strong acceptors. The key design principle is based on a different and specific role of both dihydrophenazine nitrogen donors. The resonance effect of *para*-nitrogen atom in DPPZ to the acceptor enabled to tune a zwitterionic contribution by a strength of an acceptor, forming the pre-polarized electronic structure within the polyene-like region toward the cyanine limit in the ground state. On the other hand, *meta*-nitrogen atom in DPPZ played a key role in intramolecular charge transfer to form a highly polarized electronic structure in the first excited state. Such streptomerocyanines realized considerably narrow optical and electrochemical band gaps compared to any reported DPPZ and IDD derivatives, to the best of our knowledge. Especially, a thin film of **DPPZ-IDD** with the lowest LUMO energy level exhibited an ultranarrow optical band gap close to 1 eV. Their generated excited state emitted fluorescence in visible to NIR regions in various environments. Although further improvements for higher PLQY are required, enhanced fluorescence in the aggregation state would have potential for use in theranostics.

Supporting Information

The authors have cited additional references within the Supporting Information.[S1–S9]

Acknowledgments

This work was supported by the International Cooperative Graduate Program (ICGP) provided by National Institute for Materials Science (NIMS). This work was supported by the World Premier International Research Center Initiative (WPI), MEXT, Japan. The authors thank the Czech Science Foundation Grant No. 24–10479S for the financial support. Computational resources were supplied by the project "e-Infrastruktura CZ" (e-INFRA CZLM2018140) supported by the Ministry of Education, Youth, and Sports of the Czech Republic. The authors thank the NIMS open facility for access to NIR spectrophotometer.

Open access publishing facilitated by Univerzita Pardubice, as part of the Wiley - CzechELib agreement.

Conflict of Interests

The authors declare no conflict of interest.

Data Availability Statement

The data that support the findings of this study are available from the corresponding author upon reasonable request.

Keywords: chromophore · dihydrophenazines · merocyanine · narrow bandgap · NIR emission

[1] a) N. Zhao, J. Wang, *Renewable Sustainable Energy Rev.* **2024**, *196*, 114368; b) Y. Zhang, Z. Xie, Y. Ma, *CCS Chem.* **2025**, *7*, 10.
[2] W. Liu, X. Xu, J. Yuan, M. Leclerc, Y. Zou, Y. Li, *ACS Energy Lett.* **2021**, *6*, 598.
[3] a) J. Lee, S. Song, J. Huang, Z. Du, H. Lee, Z. Zhu, S.-J. Ko, T.-Q. Nguyen, J. Y. Kim, K. Cho, G. C. Bazan, *ACS Materials Lett.* **2020**, *2*, 395; b) M. Yang, X. Tan, B. Yin, S. Kim, S. Pang, Z. Chen, X. Yang, C. Yang, Z. Liu, C. Duan, *ACS Energy Lett.* **2023**, *8*, 2641.
[4] H. Piwoński, S. Nozue, S. Habuchi, *ACS Nanosci. Au* **2022**, *2*, 253.
[5] a) C. Li, G. Jiang, J. Yu, W. Ji, L. Liu, P. Zhang, J. Du, C. Zhan, J. Wang, B. Z. Tang, *Adv. Mater.* **2023**, *35*, 2208229; b) H. Xu, Y.-Y. Zhao, Ch. Kim, G. Song, Q. Hu, H. Kang, J. Yoon, *Adv. Mater.* **2024**, *36*, 2402806.
[6] J. Mu, M. Xiao, Y. Shi, X. Geng, H. Li, Y. Yin, X. Chen, *Angew. Chem. Int. Ed.* **2022**, *61*, e202114722.
[7] a) Q. Li, Y. Guo, Y. Liu, *Chem. Mater.* **2019**, *31*, 6359; b) T. Li, G. Hu, L. Tao, J. Jiang, J. Xin, Y. Li, W. Ma, L. Shen, Y. Fang, Y. Lin, *Sci. Adv.* **2023**, *9*, eadf6152; c) Y. Chen, Y. Zheng, J. Wang, X. Zhao, G. Liu, Y. Lin, Y. Yang, L. Wang, Z. Tang, Y. Wang, Y. Fang, W. Zhang, X. Zhu, *Sci. Adv.* **2024**, *10*, eadm9631; d) H. Zhang, R. Mao, L. Yuan, Y. Wang, W. Liu, J. Wang, H. Tai, Y. Jiang, *ACS Appl. Mater. Interfaces* **2024**, *16*, 9088.
[8] a) A. Zampetti, A. Minotto, F. Cacialli, *Adv. Func. Mater.* **2019**, *29*, 1807623; b) H. U. Kim, T. Kim, C. Kim, M. Kim, T. Park, *Adv. Func. Mater.* **2022**, *33*, 2208082; c) R. Jiang, Z. Liu, T. Yang, D. Yang, D. Ma, B. Z. Tang, Z. Zhao, *Adv. Optical Mater.* **2023**, *12*, 2302034.
[9] J.-J. Wu, X.-D. Wang, L.-S. Liao, *ACS Photonics* **2019**, *6*, 2590.
[10] J. Li, J. Wang, L. Xu, H. Chi, X. Liang, J. Yoon, W. Lin, *Angew. Chem. Int. Ed.* **2024**, *63*, e202312632.
[11] a) Y. Ni, S. Lee, M. Son, N. Aratani, M. Ishida, A. Samanta, H. Yamada, Y.-T. Chang, H. Furuta, D. Kim, J. Wu, *Angew. Chem. Int. Ed.* **2016**, *55*, 2815; b) A. Mizuno, R. Matsuoka, T. Mibu, T. Kusamoto, *Chem. Rev.* **2024**, *124*, 1034.
[12] a) S. Pascal, S. David, Ch. Andraud, O. Maury, *Chem. Soc. Rev.* **2021**, *50*, 6613; b) S. S. R. Kommidi, K. M. Atkinson, B. D. Smith, *J. Mater. Chem. B* **2024**, *12*, 8310.
[13] a) N. G. Pschirer, C. Kohl, F. Nolde, J. Qu, K. Müllen, *Angew. Chem. Int. Ed.* **2006**, *45*, 1401; b) G. J. Richards, J. P. Hill, *Acc. Chem. Res.* **2021**, *54*, 3228; c) Z.-H. Wu, H. Reichert, H. Reichelt, T. Basché, K. Müllen, *Chem. Eur. J.* **2022**, *28*, e202202291; d) S. Maier, N. Hippchen, F. Jester, M. Dodds, M. Weber, L. Skarjan, F. Rominger, J. Freudenberg, U. H. F. Bunz, *Angew. Chem. Int. Ed.* **2023**, *62*, e202214031.
[14] F. Bureš, *RSC Adv.* **2014**, *4*, 58826.
[15] L. Ma, S. Zhang, J. Hou, *J. Mater. Chem. A*, **2023**,*11*, 481.
[16] A. V. Kulinich, A. A. Ishchenko, *Chem. Rev.* **2024**, *124*, 12086.
[17] a) H. Mustroph, *Dyes. Pigm.* **2022**, *208*, 110783; b) H. Mustroph, *Phys. Sci. Rev.* **2021**, *6*, 199.
[18] a) F. Würthner, *Acc. Chem. Res.* **2016**, *49*, 868; b) T. Kim, S. Kang, E. Kirchner, D. Bialas, W. Kim, F. Würthner, D. Kim, *Chem* **2021**, *7*, 715.
[19] a) T. Chatterjee, M. Mandal, S. Mardanya, M. Singh, A. Saha, S. Ghosh, P. K. Mandal, *Chem. Commun.*, **2023**, *59*, 14370; b) S. Ghosh, S. Kumar, S. Suneesh, H. Bhambri, S. K. Mandal, S. Ghosh, R. Chowdbury, P. S. Addy, *J. Org. Chem.* **2024**, *89*, 9303.
[20] S. Redon, G. Eucat, M. Ipuy, E. Jeanneau, I. Gautier-Luneau, A. Ibanez, C. Andraud, Y. Bretonnière, *Dyes. Pigm.* **2018**, *156*, 116.
[21] Q. Zhang, B. Li, S. Huang, H. Nomura, H. Tanaka, C. Adachi, *Nature Photonics*, **2014**, *8*, 326.
[22] J. Dosso, M. Prato, *Chem. Eur. J.* **2023**, *29*, e202203637.
[23] a) Q. Wan, Y. Li, K. Ding, Y. Xie, J. Fan, J. Tong, Z. Zeng, Y. Li, C. Zhao, Z. Wang, B. Z. Tang, *J. Am. Chem. Soc.* **2023**, *145*, 1607; b) J. Heo, C.-K. Lim, D. R. Whang, J. Shin, S. Y. Jeong, S. Y. Park, I. C. Kwon, S. Kim. *Chem. Eur. J.* **2012**, *18*, 8699.
[24] a) D. Karthik, Y. H. Jung, H. Lee, S. Hwang, B.-M. Seo, J.-Y. Kim, C. W. Han, J. H. Kwon, *Adv. Mater.* **2021**, *33*, 2007724; b) T. Zhao, S. Jiang, X.-D. Tao, M. Yang, L. Meng, X.-L. Chen, C.-Z. Lu, *Dyes. Pigm.* **2023**, *211*, 111065; c) D. Püschel, J. Wiefermann, S. Hédé, T. Heinen, L. Pfeifer, O. Weingart, M. Suta, T. J. J. Müller, C. Janiak, *J. Mater. Chem. C*, **2023**, *11*, 8982.
[25] L. Liu, Y. Li, H. Fu, X. Guo, Q. Wan, W. Li, B. Z. Tang, Z. Wang, *Chem. Engineering J.* **2024**, *496*, 154156.

[26] A. Vega-Peñaloza, J. Mateos, X. Companyó, M. Escudero-Casao, L. Dell'Amico, *Angew. Chem. Int. Ed.* **2021**, *60*, 1082.
[27] S. Li, M. He, X. Jin, W. Geng, C. Li, X. Li, Z. Zhang, J. Qian, J. Hua. *Chem. Mater.* **2022**, *34*, 5999.
[28] J. Xu, X. Jin, X. Wu, X. Li, C. Li, S. Li, Z. Zhang, J. Hua, *J. Mater. Chem. B*, **2024**, *12*, 6384.
[29] a) K. Pauk, S. Luňák Jr., A. Růžička, A. Marková, A. Mausová, M. Kratochvíl, K. Melánová, M. Weiter, A. Imramovský, M. Vala, *Chem. Eur. J.* **2021**, *27*, 4341; b) K. Pauk, S. Luňák Jr., A. Růžička, A. Marková, K. Teichmanová, A. Mausová, M. Kratochvíl, R. Smolka, T. Mikysek, M. Weiter, A. Imramovský, M. Vala, *RSC Adv.* **2022**, *12*, 34797.
[30] a) X. Li, S.-H. Kim, Y.-A. Son, *Dyes. Pigm.* **2009**, *82*, 293; b) C. Heichert, H. Hartmann, *Z. Naturforsch.* **2016**, *71b*, 651; c) Z. Yang, Z. Zhang, Z. Lei, D. Wang, H. Ma, B. Z. Tang, *ACS Nano* **2021**, *15*, 7328.
[31] V. D. Pokhodenko, V. G. Koshechko, A. N. Inozemtsev, *J. Chem. Soc., Chem. Commun.*, **1985**, 72.
[32] T. Okamoto, E. Terada, M. Kozaki, M. Uchida, S. Kikukawa, K. Okada, *Org. Lett.* **2003**, *5*, 373.
[33] a) X. Chen, Z. Zhao, Y. Liu, P. Lu, Y. Wang, *Chem. Lett.* **2008**, *37*, 570; b) T. Qin, R. Li, H. Jin, Y. Wang, L. Feng, *Biomater. Sci.* **2022**, *10*, 6003; c) M. Planells, N. Robertson, *Eur. J. Org. Chem.* **2012**, *26*, 4947.
[34] A. V. Kulinich, A. A. Ishchenko, *Chem. Rec.* **2024**, *24*, e202300262.
[35] A. Capobianco, R. Borrelli, A. Landi, A. Velardo, A. Peluso, *J. Phys. Chem. A* **2016**, *120*, 5581.
[36] a) A. A. Ishchenko, A. V. Kulinich, S. L. Bondarev, V. N. Knyukshto, *J. Phys. Chem. A*, **2007**, *111*, 13629; b) S. V. Shishkina, V. V. Dyakonenko, A. A. Ishchenko, A. V. Kulinich, *Struct. Chem.* **2022**, *33*, 169.
[37] F. Würthner, G. Archetti, R. Schmidt, H-G. Kuball, *Angew. Chem. Int. Ed.* **2008**, *47*, 4529.
[38] a) M. Kratochvíl, M. Ciganek, C. Yumusak, H. Seelajaroen, I. Cisařová, J. Fábry, M. Vala, S. Luňák Jr., M. Weiter, N. S. Sariciftci, J. Krajcovic, *Dyes Pigm.* **2022**, *197*, 109884; b) S. Luňák Jr., M. Weiter, M. Vala, *ChemPhysChem* **2022**, *23*, e202200252; c) K. Pauk, S. Luňák Jr., O. Machalický, F. Perdih, J. Vyňuchal, Z. Eliáš, A. Imramovský, *ChemPlusChem* **2023**, *88*, e202300310; d) M. Kratochvil, M. A. Thottappali, S. Luňák, Jr., K. Pauk, D. Rais, A. Marková, J. Pfleger, A. Imramovský, M. Vala, *ChemPhotoChem* **2023**, *7*, e202300201.
[39] a) H. Bürckstümmer, E. V. Tulyakova, M. Deppisch, M. R. Lenze, N. M. Kronenberg, M. Gsänger, M. Stolte, K. Meerholz, F. Würthner, *Angew. Chem. Int. Ed.* **2011**, *50*, 11628; b) A. Lv, M. Stolte, F. Würthner, *Angew. Chem. Int. Ed.* **2015**, *54*, 10512.
[40] S. Luňák Jr., Z. Eliáš, T. Mikysek, J. Vyňuchal, J. Ludvik, *Electrochim. Acta* **2013**, *106*, 351.
[41] S. Luňák Jr., B. Frumarová, T. Mikysek, J. Vyňuchal, *Chem. Phys. Lett.* **2013**, *570*, 50.
[42] T. Yanai, D. P. Tew, N. C. Handy, *Chem. Phys. Lett.* **2004**, *393*, 51.
[43] X. Nie, H. Su, T. Wang, H. Miao, B. Chen, G. Zhang, *J. Phys. Chem. Lett.* **2021**, *12*, 3099.
[44] W. Chen, T. Liu, J. Zou, D. Zhang, M. K. Tse, S.-W. Tsang, J. Luo, A. K.-Y. Jen, *Adv. Mater.* **2024**, *36*, 2306089.
[45] C. Zhong, D. Bialas, F. Spano, *J. Phys. Chem. C* **2020**, *124*, 2146.
[46] a) H. Suzuki, in *Electronic Absorption Spectra and Geometry of Organic Molecules*, Academic Press, **1967**, pp. 79–92; b) J. Griffiths, in *Colour and Constitution of Organic Molecules*, Academic Press, **1976**, pp. 72–75.
[47] D. K. A. Phan Huu, S. Saseendran, R. Dhali, L. G. Franca, K. Stavrou, A. Monkmani, A. Painelli, *J. Am. Chem. Soc.* **2022**, *144*, 15211.
[48] a) A. I. Ivanov, B. Dereka, E. Vauthey, *J. Chem. Phys.* **2017**, *146*, 164306; b) P. Verma, M. Tasior, P. Roy, S. R. Meech, D. T. Gryko, E. Vauthey, *Phys. Chem. Chem. Phys.* **2023**, *25*, 22689.
[49] J. Hoche, A. Schulz, L. M. Dietrich, A. Humeniuk, M. Stolte, D. Schmidt, T. Brixner, F. Würthner, R. Mitric, *Chem. Sci.* **2019**, *10*, 11013.
[50] a) C. Zhong, *Phys. Chem. Chem. Phys.* **2015**, *17*, 9248; b) C. Wang, Q. Qiao, W. Chi, J. Chen, W. Liu, D. Tan, S. McKechnie, D. Lyu, X.-F. Jiang, W. Zhou, N. Xu, Q. Zhang, Z. Xu, X. Liu, *Angew. Chem. Int. Ed.* **2020**, *59*, 10160.
[51] S. Joulaei-Zonouz, H. Wiebe, C. Prüfert, H.-P. Loock, *New J. Chem.* **2024**, *48*, 4077.
[52] F. C. Spano, *Acc. Chem. Res.* **2010**, *43*, 429.
[53] J. Gierschner, J. Shi, B. Milián-Medina, D. Roca-Sanjuán, S. Varghese, S. Y. Park, *Adv. Opt. Mater.* **2021**, *9*, 2002251.
[54] J. Mei, N. L. C. Leung, R. T. K. Kwok, J. W. Y. Lam, B. Z. Tang, *Chem. Rev.* **2015**, *115*, 11718.
[55] G. M. Sheldrick, *Acta Cryst.* **2015**, *A71*, 3.
[56] A. L. Spek, *Acta Cryst.* **2015**, *C71*, 9.
[57] M. J. Frisch, W. G. Trucks, H. B. Schlegel, G. E. Scuseria, M. A. Robb, J. R. Cheeseman, G. Scalmani, V. Barone, B. G. Mennucci, A. Petersson, H. Nakatsuji, M. Caricato, X. Li, H. P. Hratchian, A. F. Izmaylov, J. Bloino, G. Zheng, J. L. Sonnenberg, M. Hada, M. Ehara, K. Toyota, R. Fukuda, J. Hasegawa, M. Ishida, T. Nakajima, Y. Honda, O. Kitao, H. Nakai, T. Vreven, J. A. Montgomery Jr., J. E. Peralta, F. Ogliaro, M. Bearpark, J. J. Heyd, E. Brothers, K. N. Kudin, V. N. Staroverov, R. Kobayashi, J. Normand, K. Raghavachari, A. Rendell, J. C. Burant, S. S. Iyengar, J. Tomasi, M. Cossi, N. Rega, J. M. Millam, M. Klene, J. E. Knox, J. B. Cross, V. Bakken, C. Adamo, J. Jaramillo, R. Gomperts, R. E. Stratmann, O. Yazyev, A. J. Austin, R. Cammi, C. Pomelli, J. W. Ochterski, R. L. Martin, K. Morokuma, V. G. Zakrzewski, G. A. Voth, P. Salvador, J. J. Dannenberg, S. Dapprich, A. D. Daniels, Ö. Farkas, J. B. Foresman, J. V. Ortiz, J. Cioslowski, D. J. Fox. C. T. Wallingford, *Gaussian 09, Revision D.01*, Gaussian, Inc., Wallingford CT **2009**.

Manuscript received: May 29, 2025
Revised manuscript received: June 26, 2025
Version of record online: July 9, 2025